Calculated Protein and Proton Motions Coupled to Electron Transfer: Electron Transfer from Q_A^- to Q_B in Bacterial Photosynthetic Reaction Centers[†]

E. G. Alexov and M. R. Gunner*

Department of Physics, City College of New York, 138th Street and Convent Avenue, New York, New York 10031

Received November 11, 1998; Revised Manuscript Received April 27, 1999

ABSTRACT: Reaction centers from *Rhodobacter sphaeroides* were subjected to Monte Carlo sampling to determine the Boltzmann distribution of side-chain ionization states and positions and buried water orientation and site occupancy. Changing the oxidation states of the bacteriochlorophyll dimer electron donor (P) and primary (Q_A) and secondary (Q_B) quinone electron acceptors allows preparation of the ground (all neutral), $P^+Q_A^-$, $P^+Q_B^-$, $P^0Q_A^-$, and $P^0Q_B^-$ states. The calculated proton binding going from ground to other oxidation states and the free energy of electron transfer from $Q_A^-Q_B$ to form $Q_AQ_B^-$ (ΔG_{AB}) compare well with experiment from pH 5 to pH 11. At pH 7 ΔG_{AB} is measured as −65 meV and calculated to be −80 meV. With fixed protein positions as in standard electrostatic calculations, ΔG_{AB} is +170 meV. At pH 7 ≈0.2 H^+/protein is bound on Q_A reduction. On electron transfer to Q_B there is little additional proton uptake, but shifts in side chain protonation and position occur throughout the protein. Waters in channels leading from Q_B to the surface change site occupancy and orientation. A cluster of acids (GluL212, AspL210, and L213) and SerL223 near Q_B play important roles. A simplified view shows this cluster with a single negative charge (on AspL213 with a hydrogen bond to SerL233) in the ground state. In the Q_B^- state the cluster still has one negative charge, now on the more distant AspL210. AspL213 and SerL223 move so SerL223 can hydrogen bond to Q_B^-. These rearrangements plus other changes throughout the protein make the reaction energetically favorable.

The movement of charges through proteins and membranes is important in processes such as photosynthesis and respiration that convert light or chemical energy to biologically useful forms and in the ATPase and channel proteins that return ions across the membrane to do useful work. The thermodynamic penalty for moving charges out of water into proteins and membranes is well established (*1*−*5*). However, buried charges can be stabilized by movement of groups in the protein or by counterion binding (*6*). Electron transfer in cytochrome *c* oxidase is coupled to proton transfer across the membrane (*7*), while proton transfer in the ATPase (*8*) and in bacteriorhodopsin may also be accompanied by large-scale motions of protein and cofactors (*9*, *10*). However, the atomic details of each of these processes are unknown.

Bacterial photosynthetic reaction centers (RCs)[1] have provided a useful system for studying transmembrane electron-transfer proteins. There is a wealth of information about the rates and free energies, pH, and temperature dependence in wild-type and mutant protein from several bacteria (*11*−*13*). RCs from the bacteria *Rhodopseudomonas viridis* were the first integral membrane protein to have a structure solved to atomic resolution (*14*), and structures of RCs from *Rhodobacter sphaeroides* followed (*15*). Since then, higher resolution structures from *Rps. viridis* (*16*) and *Rb. sphaeroides* (*17*) have become available. These structures provide an opportunity to understand on an atomic level how the protein controls the free energy of electron-transfer reactions. With the appropriate computational tools it should be possible to evaluate the degree to which preexisting static fields (*18*), changes in protonation of nearby residues (*19*−*21*), or conformation changes (*22*, *23*) stabilize the different oxidation states of the protein.

The first steps in photosynthesis, which converts light energy into electrochemical energy, occur in RCs. Absorption of a photon by a dimer of bacteriochlorophyll (P) starts a series of electron transfers. The initial charge separation involves electron transfer from P to a bacteriopheophytin (H_L). H_L reduces the primary quinone Q_A which then passes its electron to the secondary quinone Q_B. Thus, on absorption of one photon the protein goes from a redox state where all cofactors are neutral to the $P^+Q_B^-$ redox state (*12*, *13*). This process occurs with a 98% quantum yield, separating a charge by 25 Å across the cell membrane, and results in the capture of approximately 35% of the energy of the 865 nm (1.4 eV) photon that initiates the reactions.

The electron transfer from Q_A^- to Q_B in *Rb. sphaeroides* RCs is the focus of the work presented here. In these RCs both quinones are ubiquinone-10. However, despite their chemical identity, their function is different. Electron transfer from the ubiquinone in the Q_A site to the identical cofactor in the Q_B site is favorable, with a change in free energy of −65 meV (−1.5 kcal/mol). Q_A can be reduced by H_L^- even at temperatures of 1 K, while Q_B reduction does not occur in frozen protein. Q_A accepts only a single electron and never

[†] We are grateful for the financial support of HFSO Grant RG-329/95 and NSF MCB 9629047.

* Corresponding author. Phone: (212) 650-6807. Fax: (212) 650-6940. E-mail: gunner@sci.ccny.cuny.edu.

[1] Abbreviations: P, bacteriochlorophyll dimer which is the electron donor in the reaction center protein; H_L, bacteriopheophytin near Q_A on the active L branch of the protein; UQ, ubiquinone-10; RC, reaction center; Q_A and Q_B, primary and secondary quinone electron acceptors; MCCE, Multi_Conformation Continuum Electrostatics method.

10.1021/bi982700a CCC: $18.00
Published on Web 06/09/1999

binds protons. Q_B is reduced to the semiquinone, and then it accepts a second electron and two protons to yield the final dihyroquinone product. Q_BH_2 is released from the protein with rebinding of another oxidized quinone from the quinone pool in the membrane, while Q_A is very tightly bound and does not leave the protein.

The differences between the Q_A and Q_B sites must be controlled by their surroundings. Each quinone is bound approximately 15 Å from the protein surface. Studies of site-directed mutations have identified a number of residues as being functionally important for electron and proton transfers to Q_B (see refs *24* and *25* for reviews). A number of mutations change the free energy of the electron transfer while others change reaction rates (*13*). Close to physiological rates and reaction energies can be recovered by second-site revertants (*26*−*30*).

Protons are bound to the protein in less than 200 μs following Q_B reduction in a process that is pH and salt dependent (*31*). Measurements of the pH dependence of the proton binding stoichiometry suggested that pK_a shifts of a number of ionizable groups are involved in the proton uptake (*32*, *33*). Recent theoretical work has identified several clusters of acids that dominate the response of the protein to Q_B reduction (*19*, *20*). A number of mutations slow proton delivery to Q_B (*26*, *34*−*38*). Several pathways of water-filled channels have been identified (*15*, *17*, *39*). Their importance for proton uptake has been investigated by site-directed mutations which have tried to break the hydrogen bond connectivity (*37*).

Studies of mutations focus on the role of specific residues. However, the availability of atomic structures allows analysis of how the whole protein contributes to the observed function. The electron transfer from Q_A^- to Q_B occurs on the microsecond time scale, is dependent on pH, and has significant activation energy (*40*, *41*). Standard electrostatic calculations have been applied to study the electron transfer from Q_A^- to Q_B in a rigid protein without buried waters (*19*−*21*, *42*). A picture of the regions of the protein that respond to the electron transfer between the quinones has begun to emerge. However, with the exception of the calculations by Rabenstein et al. (*21*) all have failed to reproduce the favorable free energy of electron transfer from Q_A^- to Q_B probably because these calculations failed to capture required changes in protein conformation induced by the electron transfer.

Simultaneous calculation of side-chain ionization and conformation has been attempted by a number of methods [see ref *43* and reviews (*3*, *4*, *44*)]. The earliest methods either averaged interactions between different possible side-chain atomic positions (*45*, *46*) or averaged the ionization states calculated for different structures (*47*, *48*). New methods dynamically combine conformation changes with the calculation of ionizable states (*22*, *23*). The multiconformation continuum electrostatics procedure (MCCE) has been previously described where multiple positions of hydroxyl and water protons were sampled in the analysis of the pH dependence of the ionization of acids and bases in lysozyme (*23*). Here the method has been extended to add movement of side-chain heavy atoms and water oxygens. The distribution of conformation and ionization states is determined by Monte Carlo sampling.

The MCCE method was used to calculate the free energy of electron transfer from Q_A^- to Q_B from pH 5 to pH 11 as well as the proton uptake that occurs on the formation of four different redox states of the protein. The results of the computation compare very well with the experimental data. Analysis of the results provides a picture of residues throughout the protein that change their position or charge. The mobility of waters in response to changes in the charge state of the quinones provides information about the role of different water channels. The outcome points to the importance of protein motions for stabilization of the charge on Q_B.

METHODS

Heavy Atom Positions. The structure of the reaction centers from *Rb. sphaeroides* 1aij (first molecule in the unit cell) (*17*) from the Brookhaven Protein Data Bank (*49*) provided the framework coordinates of all backbone and nonpolar side-chain atoms for the calculations. Additional heavy atom conformers were added for the 26 residues that have pairwise electrostatic interactions of more than ±0.59 kcal/mol with either Q_A or Q_B in 1aij.[2] These side-chain positions were taken from the different structures of *Rb. sphaeroides* RCs found in 1pcr (*15*), 2rcr (*50*), and 4rcr (*51*) and from the structure 1prc (*16*) of the *Rps. viridis* RCs. Each alternative rotamer was superimposed on the backbone at the appropriate position in the 1aij structure, providing five possible conformers per residue. These were screened, eliminating side chains where all atom positions differ by less than 1 Å. Of the 26 residues, 7 have five conformers, 16 have four, and 3 have three. The orientation of the terminal oxygen and nitrogen on Asn and Gln is generally not well determined in the structure (*52*). Throughout the L and M subunits an additional conformer was created for each of these residues by a 180° rotation around the terminal carbon. 1aig is an RC structure crystallized under illumination (*17*). No side chains in 1aig differ significantly from 1aij so none were added. 1aig does provide an alternative Q_B position which is included (Figure 1a).

While there is little difference between the side chain positions in the 1aig and 1aij structures, there are significant differences in water positions. Water oxygens were obtained from the two proteins in the unit cell of each structure. The two proteins in 1aij have 263 (110 buried) and 205 (89 buried) waters while in 1iag the proteins have 53 (21 buried) and 33 (15 buried) waters. All the buried waters, with less than 5 Å^2 surface accessible to a probe with a radius of 1.4 Å, are retained. Waters from different structures are then defined as being in the same site if their Lennard-Jones interactions are so large that they can never simultaneously be present in the structure (>30 kcal/mol, a distance of ≈1.75 Å between oxygens). Thus the 235 buried water oxygens can be identified with 126 sites. There are only 5 sites with waters at nearby positions in all four structures, 31 in three, 39 in two, and 51 in only one structure. Conflicts between waters in a given site are avoided by providing each water with a conformer which does not interact with the protein.

[2] Arg: L103, L217, L231, M233, M241, M247, M253, M267. Asp: L210, L213. Glu: H122, H173, L212, M232, M234, M236, M246, M263. His: L190, L230, M219, M266. Lys: H130. Ser: L223. Thr: L226; Tyr: L222.

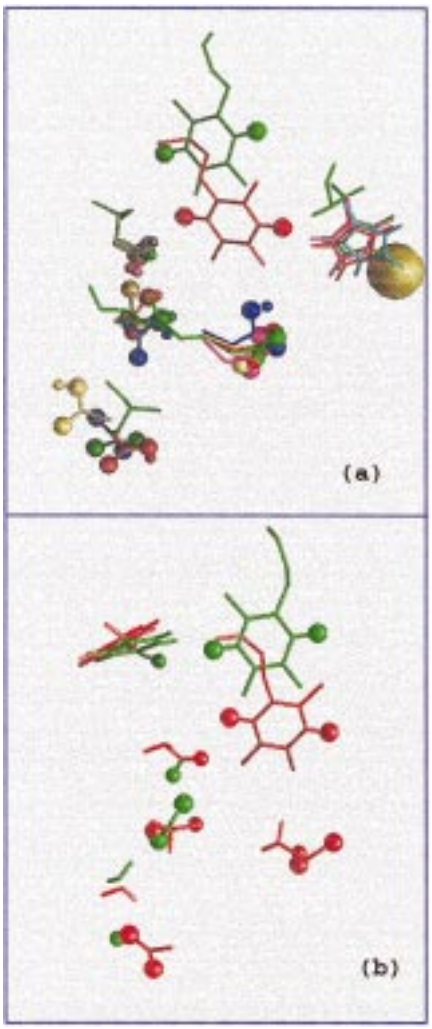

FIGURE 1: Available positions for Q_B [distal (top) and proximal (lower)]. Side-chain rotomers for (moving downward on the left) SerL223, AspL213 and GluL212, and AspL210 and (on the right) HisL190 and the non-heme iron. Oxygens are larger and hydroxyl protons smaller balls. (b) Conformation changes upon Q_B reduction. The most populated conformers in the $Q_A^- Q_B^0$ state are shown in green, while the most populated in the $Q_A^0 Q_B^-$ state are in red. The change in ionization and conformation of AspL213 and AspL210 and conformation changes of SerL223, TyrL222, and water 6 are shown.

Thus each water is allowed to leave the protein during Monte Carlo sampling.

Hydrogen Conformers. Throughout the protein each neutral His has two conformers with ND1 or NE2 protonated, and the waters, Ser, Tyr, and Thr have alternate positions for their hydroxyl protons. Hydroxyls were placed at minimum energy positions and given different ionization states of the acids Asp, Glu, and Tyr and the bases Arg, Lys, and His using the program PROTEUS[3] (*18*). PROTEUS places protons considering torsion and Lennard-Jones potentials and electrostatic interactions in a uniform dielectric constant of 20. These energies were not used in the final Monte Carlo sampling but were used only to find a set of proton conformers for further analysis. Polar protons connected by distances of less than 4 Å were minimized together. Protons were placed on side-chain heavy atom conformers and waters from each protein structure separately. With a cutoff of 2.5 Å for pairwise interactions protons were placed on the assumptions that (1) all titratable groups are ionized; (2) the bases are ionized and the acids are neutral; (3) the acids are ionized and the bases are neutral; (4) all titratable groups are neutral; (5) all titratable groups are ionized with a cutoff for electrostatic interactions of 4.5 or (6) 6.5 Å; and (7) all titratable groups are ionized as is Q_B or (8) Q_A. A maximum of eight different hydroxyl hydrogen positions were calculated for side chains and waters from each structure and up to two hydrogen positions for neutral forms of Asp, Glu, and Tyr. Proton conformers were screened so that all hydrogens for a given residue or water are separated by at least 0.2 Å. Thirty-five Ser, 19 Tyr, 29 Thr, and 19 waters have only one allowed position for their polar protons. Water sites were found to have as few as 2 possible water conformers (one oxygen with one orientation plus the option to leave the protein) and as many as 21 conformers (with four oxygens each with different hydrogen positions).

Electrostatic Calculations. The electrostatic energy of each of the conformers was calculated using the finite-difference technique to solve the Poisson−Boltzmann equation with the program DelPhi (*53*, *54*). PARSE charges and radii were used (*55*). The charges for quinones are taken from ref *20* and for all other cofactors from ref *56*. The Fe has a +2 charge, and His ligands use the PARSE charges for neutral histidines. Three focusing runs were done, giving a final resolution of 1.2 grids/Å (*57*). The dielectric constant for the protein was 4, and 80 was used for the bulk water. The ionic strength was 0.

One Delphi calculation was carried out for every conformer where the only charges on the protein are on this residue (see ref *23* for a more complete description). Each DelPhi calculation includes all side-chain and water conformers in the region that is defined to have a low dielectric constant (*23*), The extra atoms have little effect on the dielectric boundary between protein and solvent because residues on the surface are allowed to have only extra positions for protons but not for heavy atoms. The reaction field (self or solvation) energy for the charged conformer is obtained from the scaled reaction field energy (*54*). The difference between the reaction field energy of a reference compound in solution and that found for this conformer in the protein provides the loss of reaction field (desolvation) energy. The pairwise interactions with all conformers of other residues are obtained from (the potential at atoms in that other conformer) times (the charges that would be on those atoms if that conformer were populated). The M calculations, where M is the number of conformers, produce a vector of length M for each $\Delta G_{\mathrm{rxn},i}$ and a $M \times M$ array of the pairwise interactions between all possible conformers ($\Delta G_{\mathrm{el}}^{ij}$). In addition, each conformer has a pairwise electrostatic interaction with the backbone and with side chains that have no conformational degrees of freedom. This energy was summed for each conformer, resulting in a vector of length M ($\Delta G_{\mathrm{pol},i}$).

Nonelectrostatic Energies. The nonelectrostatic interactions for each conformer are the torsion energy, a self-energy term which is independent of the position of all other residues in the protein, and the pairwise Lennard-Jones interactions both with portions of the protein that are held rigid and with conformers of side chains that have different allowed positions.

[3] Programs used in these calculations are available upon request to gunner@sci.ccny.cuny.edu.

Table 1: Lennard-Jones Potentials Modified for Use in a Medium of $\epsilon = 4$

atom 1	atom 2	A (kcal mol^{-1} Å^{-12})	B (kcal mol^{-1} Å^{-12})	r_{min} (Å)	E_{min} (kcal/mol)
H	H	13.3	1.8	1.57	−0.10
H	O	400.7	33.2	1.70	−1.17
H	C	1602.7	66.4	1.91	−1.16
H	N	624.8	37.2	1.80	−0.94
heavy atom	heavy atom	40343.6	105.0	3.03	−0.12

The torsion angle energy favors the Tyr proton in the plane of the ring, the proton on neutral Asp and Glu between the oxygens (*58*), and the hydroxyl on Ser and Thr in their three energy minima (*59*−*61*). The torsion energies for polar protons were calculated using their actual torsion angles as in ref *23*. In addition, the different heavy atom rotamers have different torsion energies. However, statistical analysis of protein structures (*62*) shows that the probability for realizing each of the rotamers used here does not differ significantly. Therefore, no torsion energy was added to distinguish the heavy atom rotamers.

The pairwise Lennard-Jones interactions are given by $A/r^{12} - B/r^6$. The optimal length for hydrogen bonds when oxygen is the acceptor is 1.6−1.7 Å (*63*). Using values of A and B from X-PLOR (*64*) with PARSE charges (*65*) in a medium with a dielectric constant of 4, the distance of minimum energy is 2.3−2.4 Å. This is because X-PLOR Lennard-Jones parameters make good hydrogen bonds by electrostatic attraction when the dielectric constant is 1. Therefore, A and B for interactions between H and C, O, or N were recalculated so that the optimal distance between two participating atoms corresponds to measured values (*63*) (Table 1). For simplicity all heavy atom−heavy atom pairwise nonelectrostatic interactions used the same Lennard-Jones parameters. A cutoff of 10 Å was used. Pairwise Lennard-Jones interactions between all conformers of different residues were collected in a $M \times M$ matrix (G^{ij}_{nonel}). For each conformer, Lennard-Jones interactions with the backbone and with all side chains with no degrees of freedom were summed and added to the torsion angle energy and placed in a vector of length M ($\Delta G_{nonel,i}$).

Finally, if the number of ionized and neutral conformers differs for a given residue, this can bias the results to favor the charge state with more conformers (*23*). For example, there are two different neutral forms of His, with the proton on either ND1 or NE2, and only one form of His^+. Thus there are twice as many microstates with His^0 than His^+, adding an erroneous entropy term favoring the neutral form. Similarly, there are two positions for Q_B and only one for Q_A. However, the error introduced by this degree of overpopulation is small. If microstates with both forms of His^0 or Q_B^- had the same energy, the error would shift the equilibrium between His^0 and His^+ or between Q_B^- and Q_A^- by only $k_bT \ln 2 = 17.9$ meV. In addition, if one form of His^0 or Q_B^- is at higher energy, it will contribute less to the Boltzmann equilibrium of accepted microstates, reducing the error.

Microstate Energy. The possible states of the system were subjected to Monte Carlo sampling. A given RC microstate is made up of one conformer for each residue, cofactor, and water. The energy of microstate n (ΔG^n) is the sum of the electrostatic and nonelectrostatic energy terms:

$$\Delta G^n = \sum_{i=1}^{M} \delta_n(i)\{\gamma(i)[2.3k_bT(\mathrm{pH} - \mathrm{p}K_{sol,i})] + (\Delta G_{rxn,i} + \Delta G_{pol,i} + \Delta G_{nonel,i})\} + \sum_{i=1}^{M} \delta_n(i) \sum_{j=i+1}^{M} \delta_n(j)[\Delta G^{ij}_{el} + \Delta G^{ij}_{nonel}] \quad (1)$$

where k_bT is 0.59 kcal/mol (25.8 meV), M is the number of conformers, $\delta_n(i)$ is 1 for conformers that are present in the state and 0 for all others, $\gamma(i)$ is 1 for bases, −1 for acids, and 0 for polar groups and waters, and $pK_{sol,i}$ is the pK_a of the ith group in solution. Other terms are defined above. The limits on the summation of the pairwise interconformer terms ensure that each interaction is counted only once.

The energy of each conformer in a given microstate is always taken with respect to reference energies for this type of residue. The free energy is defined as zero when all residues have no net charges, are in their torsion minimum, have no interactions with the rest of the protein and all buried waters have been moved into bulk solvent. The conformer torsion energy is the difference from the minimum torsion energy for this residue. The loss of reaction field energy is the difference between the reaction field energy for this ionized or dipolar conformer in solution and the protein. The $pH - pK_{sol,i}$ term is the free energy difference between ionized and neutral forms in solution at this pH. Each water has an additional conformer that has no interactions with the protein, which represents the group moving into the solvent. The free energy of transferring the water into the protein was taken as 5.3 kcal/mol, which corresponds to the 1.5 mM solubility of water in cyclohexane plus the cost of opening a cavity in the protein (0.7 kcal/mol) (*66*).

Monte Carlo Calculations. There are 1726 conformers of side chains, protons, and waters. The number of microstates that make up this system is far too large to be solved by any statistical mechanical analysis that would require enumerating all states. Instead, the Boltzmann distribution of states was obtained by 40 million steps of Monte Carlo sampling (≈23 000/conformer). The state acceptance rate in the Metropolis sampling was 8%. The calculations took ≈10 h on one processor of a Silicon Graphics Origin 200. On 50% of the steps two residues changed their conformers. The second residue was chosen from conformers that interact by >1.8 kcal/mol with the first group chosen in this step of sampling. The multiple change method yields faster convergence (*20*, *67*). The outcome of the Monte Carlo calculations is the average occupancy of each conformer which is (the number of times this conformer is in an accepted microstate)/(the number of steps of Monte Carlo sampling).

The conformer occupancy was determined under conditions corresponding to different experimental conditions. The pH of the system was varied by changing the pH term in eq 1. The redox state of the protein was then fixed for different simulations. In the ground state calculations all microstates have only neutral P, Q_A, and Q_B. A calculation of the protein in the $P^+Q_A^-$ state requires that all microstates have the P^+ and the Q_A^- conformers rather than P^0 and Q_A^0. Separate Monte Carlo calculations were carried out for seven redox states (ground, $P^+Q_A^-$, $P^+Q_B^-$, $P^0Q_A^-$, $P^0Q_B^-$, $P(Q_A \text{ or } Q_B)^-$, and $P^+(Q_A \text{ or } Q_B)^-$ at seven different pH's (from 5 to 11). In the $P(Q_A \text{ or } Q_B)^-$ or $P^+(Q_A \text{ or } Q_B)^-$ calculations all

microstates have either Q_A^- or Q_B^- but never have both quinones reduced.

MCCE Method. The MCCE method differs from standard electrostatics calculations in several ways. Standard electrostatic calculations consider only a single structure for all heavy atoms and polar protons (*4*). In contrast, X-ray and neutron diffraction studies show that protein structures are heterogeneous (*59*, *60*, *68*). MCCE allows for alternative positions for side-chain heavy atoms, hydroxyl protons, and waters. In addition, structures can change if the pH or redox state differs from that of the initial crystal structure. While the current implementation of the method does not allow for motions of the backbone or of surface side chains, the MCCE method provides for a limited but still significant degree of protein flexibility.

In the work presented here initial rotamers were derived from several different crystal structures. However, standard rotamer libraries can be used. The set of starting conformers will affect the outcome of the calculations. Particular positions may be overpopulated, bad conformers included, or specific low-energy positions ignored. As described above overpopulation only yields significant errors if the distribution of states is very uneven, which is not the case here (see ref *23*). Including bad conformers, such as side-chain positions which overlap with the backbone, also does not raise serious problems since the high energy of microstates that include these positions means that they are never populated. Poor initial choices increase the size of the calculation but should not affect the outcome. However, if a good conformer is missing, then the system cannot find the lowest possible energy. In the Results section it will be seen that one conformer of Asp (L213) can make a good hydrogen bond with a Ser (L223) which influences its own ionization state, the ionization state of a Glu (L212), and the stability of the ionization of Q_B, the alternate hydrogen acceptor from the Ser. Thus, the method is most vulnerable to missing conformers and still requires testing against experimental data as described here.

The MCCE method can analyze a system as large as RC because the state energies are built up of only self and pairwise energies. This places limitations on allowed conformations. There can be no changes in the backbone as these would require coupling the positions of several residues. Also, only changes that do not make a significant difference in the boundary between the protein and water are allowed. Thus, if residue C changes the protein surfaces in its different allowed conformers, the electrostatic interaction between residues A and B can be screened differently by each conformation of residue C. This is not allowed. However, this paper considers the response of the protein to changes in ionization of buried redox cofactors. While surface residues can have a wide range of positions, they are exposed to the solution and their impact on the electrostatic potential inside the protein is very small. In contrast, while charges or dipoles in the interior are constrained by the protein packing, small changes in their orientation can affect other residues at a significant distance. Therefore, only buried residues have heavy atom side-chain conformers and only buried waters are considered. Surface residues are only allowed to change ionization state and polar proton positions.

Dielectric Constant in the MCCE Method. The dielectric response in the MCCE method is complex. In a standard continuum electrostatics calculation one dielectric constant is assigned to the protein and another, higher value to the solvent. However, the reaction field energy of individual charges and pairwise interactions between charges depend on the position of each charge relative to the surface. Interactions between sites without flexibility are determined by this procedure in the MCCE method. The MCCE method retains a value of 4 as the dielectric constant of the protein despite the addition of explicit atomic motions. The primary reason is that many atoms are not allowed to move so their motion must continue to be included as an averaged response. For example, the response of the backbone dipoles yields an average dielectric response of 4 (*69*), which must be treated in the dielectric constant since these atoms remain fixed. The PARSE charge set used here was parametrized with a solute dielectric constant of 2 (*55*). However, comparison of pK_a calculations in proteins with PARSE charges shows small differences in the results with $\epsilon = 2$ or 4 (*70*).

It has been shown that a dielectric constant of 4 in the static protein structure is insufficient to obtain a good match to experimentally observed pK_a's in proteins (*71*). The calculated results at $\epsilon = 4$ can be improved by using a detailed charge distribution for the side chains of both ionized and neutral forms of titratable groups (*67*, *72*, *73*). This is incorporated in the MCCE method. However, better results for the static protein can still be obtained with a value of ϵ closer to 20 (*70*, *71*). The use of a single, large dielectric constant provides no information about the groups that move, and it assumes that the response to changing charges is the same throughout the protein. The addition of explicit motions of charged groups and dipoles in the MCCE calculations will increase the effective dielectric constant. However, here the response in each region of the protein is dependent on the protein structure. The effect of the MCCE method on the dielectric response of the protein has not yet been fully characterized. Preliminary results show that polar hydrogen motions increase the effective local dielectric constant but have little effect on the average dielectric constant for the protein as a whole (*23*). Molecular dynamics simulations suggest that the motions of charged residues included here should have a larger impact (*74*−*76*).

Calculations of the Free Energy Difference between $Q_A^-Q_B$ and $Q_AQ_B^-$ (ΔG_{AB}). These calculations do not provide the total energy of the system. Many terms for the parts of the protein without conformational flexibility are not included since they change the energy of all microstates by a constant amount. In addition, the microstate energy formula (eq 1) should provide *H*, the Hamiltonian of the system which would include the kinetic energy. However, the kinetic part of the Hamiltonian contributes a constant amount to the free energy and entropy of the system (*77*) and so will not affect the energy differences discussed here.

Method 1: Calculating ΔG_{AB} from the Difference in State Energies. The free energy difference between RCs with Q_A^- and with Q_B^- (ΔG_{AB}) can be obtained from the difference in the free energy of the Boltzmann distribution of microstates with Q_A^- and with Q_B^-. The free energy of the reaction will reflect the changes throughout the protein since the relative energy of all ionization states and dipole orientations will change in response to the quinone charge.

The free energy of a state X can be calculated from the microstate energies G_n (eq 1) as described by Shellman (*78*):

$$G_X = -k_b T(\ln \sum_{n=1}^{\Omega} \exp(-\Delta G^n(X)/k_b T)) \quad (2)$$

The summation should run over all possible microstates (Ω). Thus the state $Q_A^- Q_B$ (X = A) considers all microstates which include Q_A^-, while G_B is the energy of $Q_A Q_B^-$ where all microstates have Q_B^-. The expression in the outer parentheses is the logarithm of the partition function. The partition function cannot be determined explicitly because the number of states is too large. However, if the Monte Carlo sampling procedure accepts all thermally accessible states, then collecting these microstate energies in the sum should yield a value close to the true value of G_X (*79*). This method assumes that states that are never accepted are at such high energy that they add a negligible amount to the energy. Only distinguishable energies found on each step were added so each microstate is included only once.

The actual microstate energies (ΔG^n) were found to be too negative to allow numerical compution of $\exp(-\Delta G^n/k_b T)$. To avoid this problem, the minimum microstate energy was determined in a Monte Carlo run for a given redox state and pH, and this was defined as the reference energy. This was subtracted from each new microstate energy before the exponential was calculated. The free energy of the Q_A^- to Q_B electron transfer is then

$$\Delta G_{AB} = G_B - G_A \quad (3)$$

The same reference energy was used for both calculations. For each redox state (Q_A^- or Q_B^-) the lowest value of G_X from three runs was used to calculate ΔG_{AB}. An estimate of the standard deviation was obtained from $G_B - G_A$ for three individual runs.

Method 2: Calculating ΔG_{AB} from the Equilibrium Constant. Rather than calculating the state energies of Q_A^- and Q_B^-, the free energy difference between a product (Q_B^-) and reactant (Q_A^-) can be obtained from the equilibrium constant.

$$\Delta G_{AB} = -k_b T \ln K_{eq} = -k_b T \ln \frac{\rho_B}{\rho_A} = -k_b T \left[\ln \frac{\sum_{n=1}^{\Omega} \delta_n(B) \exp(-G_n(B)/k_b T)}{Z} - \ln \frac{\sum_{n=1}^{\Omega} \delta_n(A) \exp(-G_n(A)/k_b T)}{Z} \right] = G_B - G_A \quad (4)$$

If all states could be enumerated, the fraction of states with either Q_A^- or Q_B^- in the Boltzmann distribution would be

$$\rho_X = \frac{\sum_{n=1}^{\Omega} \delta_n(X) \exp(-G_n(X)/k_b T)}{Z} \quad (5)$$

where ρ_X is the probability of finding the electron on Q_X and $\rho_A + \rho_B = 1$. If Monte Carlo sampling is carried out with all microstates containing either Q_A^- or Q_B^- but never both, the probability of finding Q_A^- and Q_B^- is ρ_A and ρ_B. The ratio of probabilities reflects the relative energy of the ensemble of microstates with either quinone reduced (*19*). Since the relative energy of microstates with Q_A^- or Q_B^- depends on the conformer distributions of all residues in the protein, the probability of either quinone being reduced is coupled into the appropriate changes in the protein.

Calculations of the free energy were run three times starting from different seeds for the random number generator. The results were averaged and the standard deviation was calculated.

Method 3: Calculating the pH Dependence of ΔG_{AB} from the Proton Uptake at Each pH. If Δq protons are bound from the solution on electron transfer, the reaction will become less favorable as the pH increases (*32*, *78*). The change in ΔG_{AB} with pH is

$$\Delta G_{AB}(pH) = \Delta G_{AB}(pH = pH_0) + k_b T(\ln 10) \int_{pH_0}^{pH_1} \Delta q(pH)\, dpH \quad (6)$$

where $\Delta G_{AB}(pH = pH_0)$ is taken to match the free energy calculated by methods 1 and 2 at pH = 7. Δq(pH) was calculated at each pH (see next section). The integral in eq 6 was estimated by a sum of Δq's at discrete pH's.

Calculation of Proton Uptake Coupled to the Electron-Transfer Reaction. If the reduction of either quinone results in a change of protonation states of titratable residues, this can cause a change in the net charge of the protein. To calculate this effect, separate Monte Carlo sampling runs were carried out (1) in the ground state where both Q_A and Q_B are neutral, (2) with $P^+Q_A^-$, (3) with $P^0Q_A^-$, (4) with $P^+Q_B^-$, and (5) with $P^+Q_B^-$. The number of titratable protons bound is

$$\langle q_{tot} \rangle = \langle \sum_{i=1}^{M} \gamma_i p_i \rangle \quad (7)$$

where ρ_i is the average occupancy of ith conformer found by Monte Carlo sampling and γ_i is +1 for neutral acids and ionized bases and 0 for all other conformers. The difference between the number of bound protons can then be calculated for any two states. For example, the proton uptake going from the ground state to the Q_A^- state is

$$\Delta q(\text{ground} \rightarrow Q_A^- Q_B) = \langle q_{tot,Q_A^- Q_B} \rangle = \langle q_{tot,ground} \rangle \quad (8)$$

RESULTS

The calculations presented here subject side-chain atomic positions and ionization states and buried water positions and site occupancy to Monte Carlo sampling in the ground state where all cofactors are neutral and in the $P^+Q_A^-$, $P^+Q_B^-$, $P^0Q_A^-$, and $P^0Q_B^-$ states from pH 5 to pH 11. This provides the Boltzmann distribution of allowed conformations of RCs in the five redox states as a function of pH. The conformer distribution in the ground state at pH 7 will be described in detail. The changes in amino acid ionization and atomic position that occur in the different redox states at different pH's will then be described. The experimental

values for the free energy of the electron transfer from Q_A^- to Q_B and for the uptake of protons from solution when the protein goes from the ground state to any of the four other redox states will then be compared with the values obtained here.

RCs in the Ground State at pH 7. The Monte Carlo sampling allows all Asp, Glu, Arg, Lys, and Tyr and the His that are not direct ligands to cofactors to be neutral or ionized. In the physiological pH range (pH 7−8) all Tyr and His are found to be neutral; Lys and Arg are fully ionized; Asp and Glu are also ionized with the following exceptions: GluH94, GluL212, and GluM236 are fully protonated and AspL210 and GluM95 are partially protonated. GluH94, in a loop near the L subunit, and GluM95, at the periplasmic surface, have interactions of less than 0.59 kcal/mol with any cofactor or any functionally important residue and so will not be discussed further. GluL212, GluM236, and AspL210 are near the Q_B site and so will be considered in more detail below.

In this protein 7 Asp (26% of all Asp's), 14 Glu (44%), 2 Lys (9%), and 17 Arg (55%) are calculated to have lost sufficient reaction field (i.e., solvation) energy to shift their pK_a's by at least 5 pH units (6.8 kcal/mol). This loss of favorable interactions with water destabilizes the charged form of both acids and bases. The observation that most acidic and basic residues are ionized *in situ* shows that dipoles and other charges in the protein are arranged to compensate for the loss of reaction field energy.

Distribution of Heavy Atom Rotamers: Side-Chain Conformer Distribution in the Protein. The PDB file 1aij (*17*) provides the starting coordinates for the calculation. Throughout the protein most hydroxyl side chains and water protons have several possible positions, neutral His can be protonated on ND1 or NE2, and Asn and Gln can exchange the position of the terminal O and N. In addition, 26 residues near Q_A and Q_B have different heavy atom rotamers that are derived from the *Rb. sphaeroides* RC PDB structures 1aij (*17*), 1pcr (*15*), 2rcr (*80*), and 4rcr (*51*) and the *Rps. viridis* structure 1prc (*16*). The backbone and heavy atom positions of all other residues are fixed in their positions in the 1aij structure.

The distribution of side-chain conformers from the four different structures in the ground state at pH 7 was calculated. The 1aij conformers were the most populated, not unexpected since the backbone and surrounding nonpolar residues are from this structure. However, more than 50% of the populated conformers come from other structures with 30% derived from 1pcr. Very few conformers from the *Rps. viridis* structure 1prc were populated. This may reflect the differences between *Rps. viridis* and *Rb. sphaeroides* RCs which have 59% homology for the L subunit, 50% for the M subunit, and 39% for the H subunit (*81*). However, the connection with the parent structures may not be very significant since the surroundings of all introduced rotamers have changed. Thus, the depletion of the 1aij conformers does show that there is room for different side-chain positions in the protein while the identification with specific parent PDB files may be simply a convenient identifier for these other rotamers.

The basic RC structure is of protein frozen for crystallography in the dark in the ground state. In addition, there is a second structure of protein frozen in the light in the $P^+Q_B^-$ state (*17*). The most significant difference between the light (1aig) and dark (1aij) structures is the position of Q_B. In the dark structure the quinone is in a distal position, 8.5 Å from the iron that lies between Q_A and Q_B. In the light the quinone is found 2 Å closer to Q_A, 7 Å from the iron. The distal quinone headgroup lies in the position occupied by the inner quinone's tail (Figure 1a). The inner quinone site is partially occupied by 4 to 5 waters in the 1aij structure. Both quinone positions are allowed, but the waters were removed from the inner site. In the ground state at pH 7 the distal site is occupied in 20% of the accepted microstates and the inner site in 80%. The neutral quinone in the inner site has slightly better interactions with backbone dipoles (0.6 kcal/mol) and with the iron (0.6 kcal/mol).

Distribution of Conformers. In the ground state at pH 7, of the 692 conformers of the 389 side chains with alternative positions and charges 12.4% are present in >99.9% of all accepted microstates. However, most of these conformers are in residues with limited degrees of freedom. Thus, 83 are polar residues with only a single conformation while 96 are the ionized form of acids and bases without additional rotamers. If these are removed, only 2% of the conformers are always occupied. Thus, most residues with degrees of freedom are present in a distribution of positions.

There are 550 conformers which are present in <0.1% of accepted microstates representing 32.5% of the total choices. Of these 143 are neutral acids and bases, including their heavy atom and polar proton rotamers which are inaccessible at pH 7. There are 407 other unutilized conformers. Some are poor initial choices, due to overlap with rigid regions of the protein. Others could only be discarded through the Monte Carlo sampling.

Thus, 55.1% of all conformers have some fractional occupancy at pH 7 in the ground state. Thirty-nine residues have one conformer with occupancy between 5% and 95%, 133 have two, 41 have three, 8 have four, and 2 have five conformers. The Monte Carlo sampling shows a protein with many states with similar, accessible energies with different side-chain positions.

Water Conformations. Much of the conformational flexibility is contained in the waters as 1034 of the 1726 total available conformers represent different water oxygen and hydrogen positions. The 1aij and 1aig structures leave significant uncertainty in the positions of waters in the protein. Combining waters from these files provides 265 oxygen positions in 126 water sites. Different proton positions on the same oxygen change the water dipole orientation. Different oxygen positions represent a translation of the water within the site. Waters also have a degree of freedom unavailable to the side chains: they can leave the protein. The water is treated as partitioning out of the bulk water into the protein site with a free energy of transfer of 5.3 kcal/mol. Calculations where this value was varied are described below.

With a 5.3 kcal/mol penalty for transfer out of bulk water, 61 waters are distributed into the 126 identifiable sites in the protein. This varies negligibly with pH, ranging from 61.4 and 61.7 between pH 5 and pH 11. The occupancy of each site is the sum of the probabilities of all oxygens and their associated protons that are too close together to be allowed in the same structure. Sites with oxygens in three or four crystal structures have larger average occupancy than sites where waters were found in fewer structures. The sites

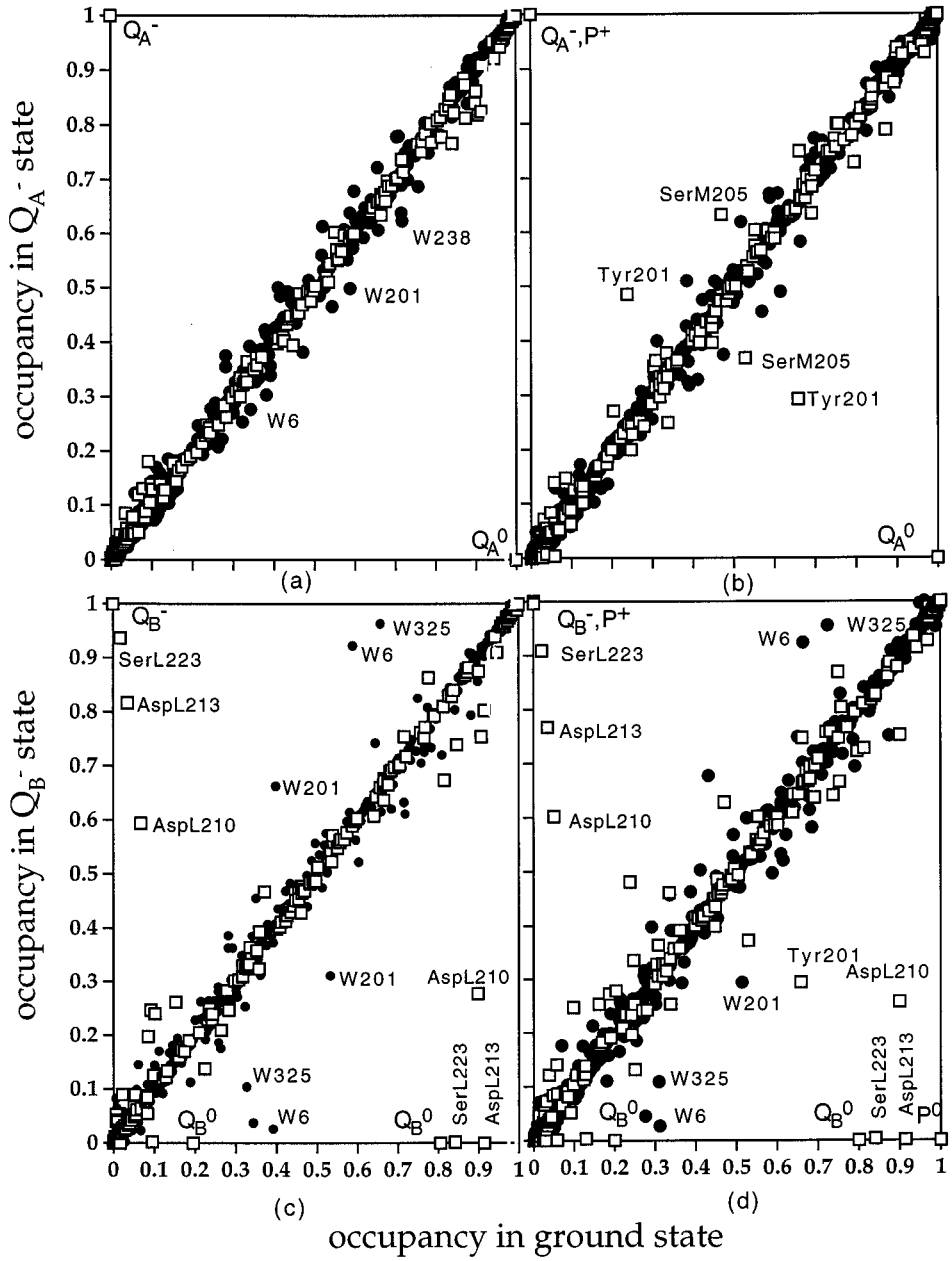

FIGURE 2: Occupancy of the conformers in the ground state plotted against the occupancy in the (a) $P^0Q_A^-$, (b) $P^+Q_A^-$, (c) $P^0Q_B^-$, or (d) $P^+Q_B^-$ states at pH = 7. Squares represent protein conformers and solid dots water conformers. The points on the diagonal do not undergo conformation changes while points to the right of the diagonal lower their occupancy and points to the left increase their conformer occupancy upon quinone reduction.

with an oxygen in only one crystal structure are 35% occupied, those with two oxygens 55% occupied, and those with three oxygens 68% occupied. There are only five sites with four oxygens, and these are 65% occupied.

As with the distribution of the side chains, water positions tend to be distributed among available conformers. In the ground state at pH 7 only 1.1% of the conformers are found in >99.9% of the accepted microstates while 17.2% of the proposed water conformers are found <0.1% of the time. Although the average occupancy of the water sites is about 50%, only a single water oxygen position has no probability of being found in the protein and all water sites are occupied in some accepted microstates.

Changes in the Protein on Reduction of Q_A: the $Q_A^-Q_B$ State. The distribution of the ionization states of acids and bases and the atomic conformers of side chains and waters were calculated with reduced Q_A. Thus, every allowed microstate in this Monte Carlo sampling must contain Q_A^-. Calculations were also carried out in the redox state $P^+Q_A^-$. There are only small differences between Q_A^- and the ground state for any residue or water. This can be seen in Figure 2a, which plots each conformer's probability in the ground state against its occupancy in the Q_A^- state at pH 7. Conformers on the diagonal do not change occupancy. Those on the right of the diagonal are less probable in RCs with Q_A^-, while points on the left are more populated in ground state RCs. The deviation from the diagonal is minimal near conformer probabilities of 0 or 1 where there are larger energy differences between conformers. Most off-diagonal elements are residues with several conformers with similar occupancy and thus comparable energies. No residue changes ionization state by more than 2%. The average population

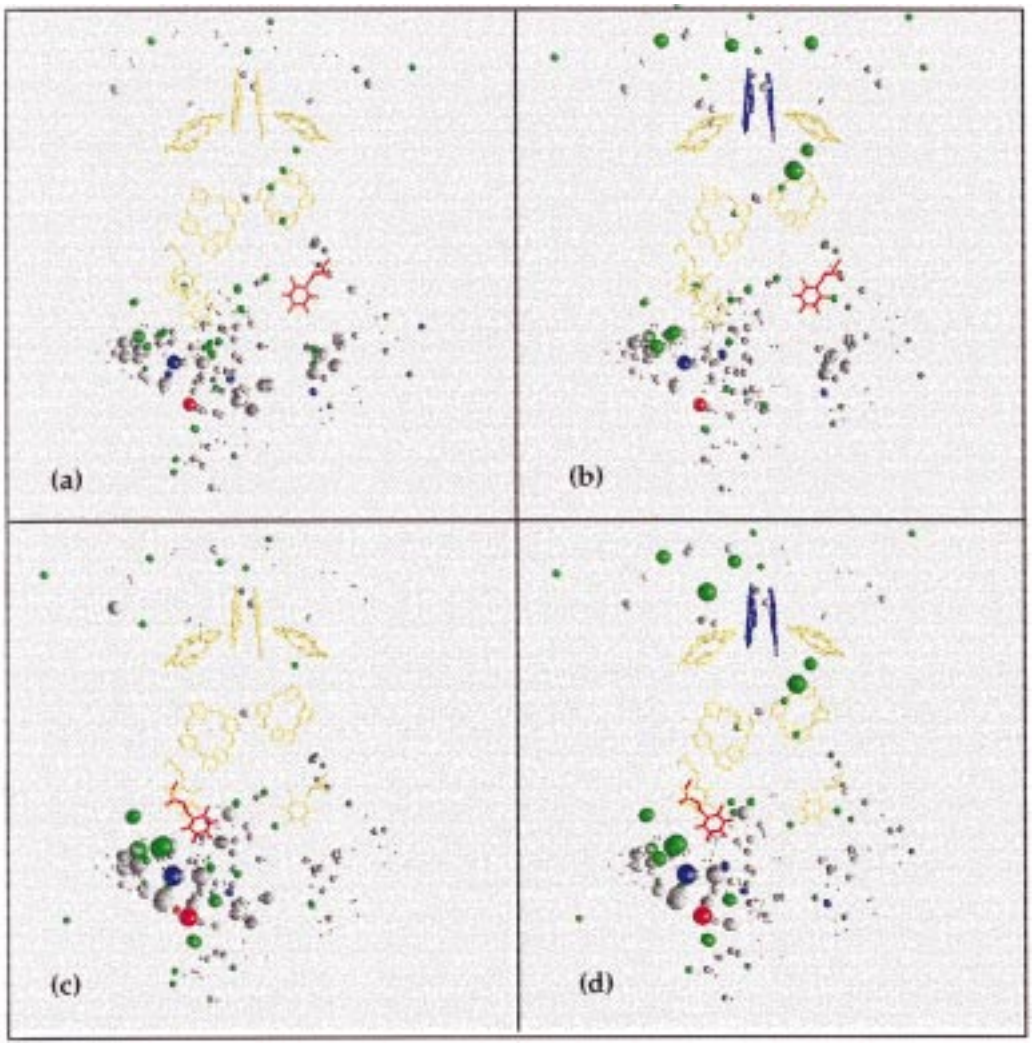

FIGURE 3: Spatial distribution of the conformer occupancy changes upon quinone reduction in (a) $P^0Q_A^-$, (b) $P^+Q_A^-$, (c) $P^0Q_B^-$, or (d) $P^+Q_B^-$ states at pH = 7. Each residue undergoing a change in its conformer distribution is shown as one ball, and the size of the ball is proportional to the relative magnitude of the change. All waters are shown; the smallest balls are waters which do not change conformation. Slightly larger balls represent waters and residues changing their conformer distribution by less than 5% from that found in the ground state, medium balls represent changes larger than 5%, and the largest balls represent changes greater than 20%. Waters are in gray, polar and charged groups that change position are in green, residues becoming more negative are in red, and residues becoming more positive are in blue. In panels c and d the large blue ball represents protonation of AspL213 upon Q_B reduction, and the large red ball shows ionization of AspL210. The hydroxyl reorientation of SerL223 and the AsnM44 dipole reorientation are shown by the large green balls to the left of the quinone. Waters within several water channels both parallel and perpendicular to the membrane surface which undergo conformation changes are seen.

of the side-chain conformers taken from the 1pcr structure increases by several percent, reducing the occupancy of the conformers from 4rcr. The position of Q_B remains 20% in the outer and 80% in the inner binding site. Many water conformers change their occupancy by up to 10%. The average total water occupancy decreases from 61.3 to 60.6, implying that on average 0.7 water leaves the protein. The ionization of P^+ causes additional conformation changes of polar residues and waters near P^+ including microdipole reorientation of TyrM210 (Figure 2b) (*18, 82*). At pH 7 there are no significant changes in side-chain ionization states in response to P oxidation.

Changes in ionization and conformation that occur upon the formation of Q_A^- at pH 7 are visualized in Figure 3a,b. The changes near Q_A and Q_B are relatively independent of the ionization state of P. There are no changes in residue ionization near Q_A. Nearby waters 19, 82, 409, and 289 [numbering from 1aij (*17*)] do change conformation slightly. However, most of the changes are found near Q_B. The largest changes were calculated for waters 6, 325, 238, and 201. In addition, AsnM44 and SerL223 undergo conformation shifts and there can be small changes in ionization of AspL213 and GluL212. The changes on Q_A reduction are sufficiently small that some details vary between individual Monte Carlo simulations. Thus, AspL213 and GluL212 are very close together and so have one proton between them in the ground and Q_A^- states. Individual simulations found GluL212 between 7% ionized to fully neutral in the ground state, with L213 between 93% and 100% ionized. L212 is always fully protonated and L213 ionized when Q_A is reduced. Thus, some simulations show a small proton transfer from L213 to L212 when RCs go from the ground state to the Q_A^- state.

Changes in the Protein on Reduction of Q_B: the $Q_AQ_B^-$ State. Calculations at pH 7 with the protein in the Q_B^- or $P^+Q_B^-$ states show that changes occurring upon Q_B reduction are significantly larger than upon Q_A reduction (Figures 2c,d

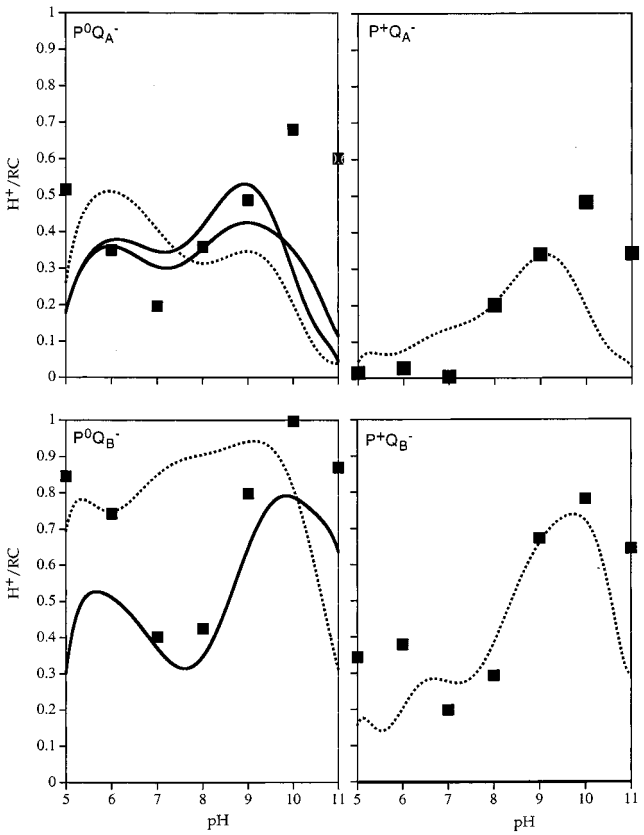

FIGURE 4: Changes in proton binding when the protein goes from the ground state to the four different redox states calculated with eq 8. Points: calculated values. Experimental data taken from ref *33* (broken curve) and ref *32* (solid curve).

and 3c,d). There is a decrease of ≈5% in the population of side-chain conformers from 1pcr while those from 4rcr and 2rcr increase by 3% and 6%, respectively. Q_B reduction causes ionization and conformation changes of as much as 95% for individual residues. Q_B^- itself is now found only in the inner binding site. All residues that undergo large changes are near Q_B. There is a shift in a proton from AspL210 to AspL213. In addition, there is reorientation of SerL223 and AsnM44. The water 6 site (the 1aij numbering is used for waters) which connects L210 and L213 (*17*) has its occupancy reduced by 56%. This change propagates through a channel, parallel to the membrane, with four water sites ending at water 281. Waters in a channel perpendicular to the membrane, which starts with water 325, near AspL213 and leads to the surface, change conformation. Thus, the calculations show at least two proton pathways that can deliver protons toward Q_B. In addition, there is another channel parallel to the membrane that connects water 6, via the side chain of ArgL217, to water 42 and then to the surface. On Q_B reduction the Arg changes its atomic position but not its ionization state, and most of the members of the channel change position. As will be seen, these conformer changes are required for the reduction of Q_B to be energetically favorable.

Proton Uptake. The stoichiometry of proton binding from solution was calculated as the protein goes from the ground state to the four oxidation states $P^+Q_A^-$, $P^0Q_A^-$, $P^+Q_B^-$, and $P^0Q_B^-$ (Figure 4). Proton uptake (or release) is the difference between the probability of each acid and base being ionized in the ground state and the new redox state (eq 8). The calculated proton uptake from pH 5 to pH 11 for the four redox states is in good agreement with the experiments with the best results found between pH 7 and pH 9 (Figure 4).

For all four changes in RC redox state, the maximum proton uptake occurs between pH 9 and pH 10. There is a peak in the proton uptake between pH 5 and pH 6 which is significantly diminished when P is oxidized. For all four reactions there is proton uptake, but it represents less than one proton per RC. Thus, when $P^0Q_A^-$ or $P^0Q_B^-$ is formed, the redox change adds a negative charge to the protein which is not fully compensated by proton uptake. When $P^+Q_A^-$ or $P^+Q_B^-$ is formed, there is no net change in protein charge and yet still protons are bound. Where available, data are shown for experiments in low (*32*) and high (*33*) salt. The largest difference is for formation of $P^0Q_B^-$ from pH 5 to pH 9 where there is significantly more proton uptake in high salt. The calculations, which assume zero ionic strength, are in better agreement with the low salt measurements.

Proton uptake is dispersed over several groups especially at low and high pH where many acids and bases are fractionally ionized. Most residues contribute very much less than one proton to the average number of protons bound to RC. Assuming a standard Henderson−Hasselbach dependence of protonation on pH, residues participate most at pH's near their pK_a's in the protein. For example, an interaction with P^+ that shifts a pK_a from 4.0 to 3.9 will cause 0.06 H^+/RC to be released at pH 4. A pK_a shift to 4.1 would cause uptake of 0.06 H^+/RC. As will be described below, many of the more important acids do not follow this simple relationship. However, it is not a bad approximation of the behavior of the more distant residues that contribute to proton binding at low and high pH.

At low pH (5−7) approximately 16 ionizable groups each take up or lose 0.01−0.05 H^+/RC on formation of Q_A^-. These groups continue to bind protons when $P^+Q_A^-$ is formed, but the net proton uptake is diminished by the fractional proton release by AspL155 and AspM184 near P. The diminution of proton uptake at low pH when $P^+Q_B^-$ rather than $P^0Q_B^-$ is formed is also due to proton release by the same acids near P. At high pH (>10) the proton uptake is dispersed over several Arg and Tyr, which are slightly less likely to be protonated in the ground state. The oxidation state of P has less impact on the proton uptake above pH 10 than it does below pH 6. Thus, acids have a larger response than bases to the charge on P.

The major differences between calculation and experiment are found at pH's less than 6 and greater than 10. For example, at pH 5 when $P^0Q_A^-$ is formed, the proton uptake is calculated to be 0.5 H^+/RC in contrast to the measured value of 0.2−0.3 H^+/RC. This arises because many groups begin to change their ionization at these pH's. Thus, the sum of small errors yields the overestimate of proton uptake. An uncompensated charge on the quinone produces an accumulation of substoichiometric proton binding at distant residues. When P is oxidized, the total charge of the protein does not change so errors from distant sites are smaller. At high pH an underestimate of the pK_a of ArgM228 which has begun to deprotonate in the ground state causes much of the overestimate of proton binding. Proton binding by M228 can reach as high as 0.38 H^+/RC (pH = 11 with $P^0Q_B^-$).

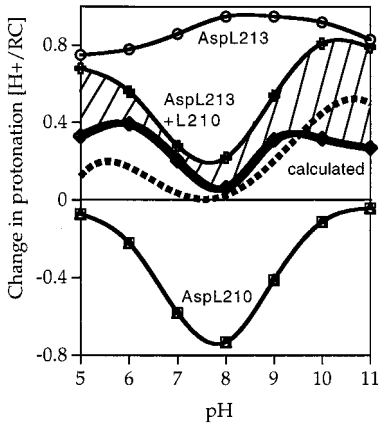

FIGURE 5: Proton uptake/release upon Q_A^- to Q_B electron transfer. Experimental data are shown as a broken curve, and all other curves are labeled. The region between zero and the bold calculated line represents protons taken up from solution. The shaded region represents protons released into the cluster by the protein. The AspL213+L210 line represents protons bound by these two groups in the cluster. The L210 line below zero represents protons released by L210.

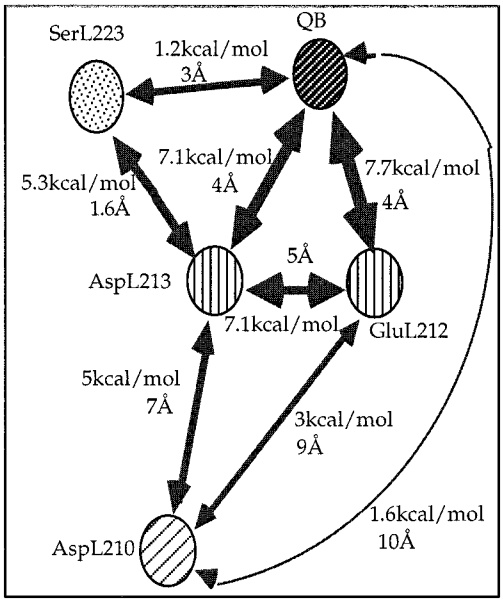

FIGURE 6: Average distances and interaction energies among the ionized form of the residues within the cluster.

Acidic Cluster near Q_B: Electron Transfer at Physiological pH's. At high and low pH a substantial fraction of a proton/RC is bound from solution, and there is more proton binding on formation of Q_B^- than Q_A^-. In contrast, at physiological pH proton uptake is approximately 0.2 H^+/RC for formation of either the Q_A^- or Q_B^- states. Thus there is almost no proton binding as the electron moves from Q_A^- to Q_B (Figure 5). Instead, a cluster of residues near Q_B (Figure 1) changes ionization and side-chain orientation. These groups can be identified as falling well off the diagonal in Figure 2c,d. Focusing the analysis on the behavior of AspL210, GluL212, AspL213, and Ser L223 provides a simple model of how the protein responds to Q_B reduction.

The pairwise energies of interaction among the ionized forms of AspL210, GluL212, and AspL213 are shown in Figure 6. Each of these residues has several heavy atom conformers so the average interactions and distances are given. AspL213 and GluL212 interact very strongly with

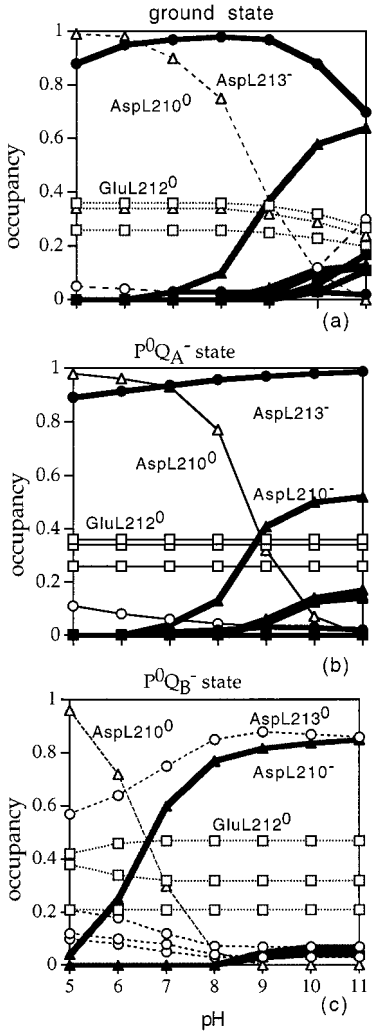

FIGURE 7: Titration of conformers within the cluster. Bold curves show the occupancy of ionized conformers and light curves the occupancy of neutral conformers. Panels: (a) ground state; (b) Q_A^- state; (c) Q_B^- state.

each other. These two acids have almost identical interactions with Q_B, while AspL210 is further away. AspL210 is closer to AspL213 than to GluL212. In addition, SerL223 can hydrogen bond to L213 or to Q_B.

The pH dependence of the heavy atom conformer occupancy and ionization states of the three acids in the cluster in the ground RC state is shown in Figure 7a. The pH dependence of each of these residues is quite anomalous. Thus, AspL213, which is mostly ionized by pH 5, begins to become reprotonated above pH 10. AspL210 is not half-deprotonated until pH 8.5, and GluL212 begins to become ionized above pH 8 but appears to reach a plateau at pH 10. This behavior is a result of strong interactions among these residues, strongest between GluL212 and AspL213. The ionization of both AspL213 and GluL212 would increase the energy of the system by approximately 7.1 kcal/mol (Figure 6). Therefore, one is ionized and one protonated throughout the pH range shown. In this calculation the proton is mostly associated with GluL212, but as described above some Monte Carlo runs suggest that GluL212 is partially ionized (7%) at physiological pH in the ground state. The proton binding by GluL212 when Q_A is reduced or by AspL213 at high pH (Figure 6) does not represent proton

Table 2: Comparison of the Structures Used and Some Results Obtained in Different Calculations of the Electron Transfer from Q_A^- to Q_B

Rb. sphaeroides	this study	ref *42*	ref *19*	*Rb. viridis*	ref *20*	ref *21*
GluL212[a]	0%	100%	70%	GluL212[a]	20%	0%
AspL213[a]	95%	60%	10%	GluH177[a]	80%	100%
AspL210[a]	5%	40%	70%	GluM234[a]	75%	75%
total charge	−1.0	−2.0	−1.5		−1.75	−1.75
water model	explicit, flexible waters	continuum dielectric	continuum dielectric		continuum dielectric	continuum dielectric
crystal structure	1aij	4rcr	4rcr		2prc	1prc
changes in structure	extra side chains	none	none		none	Q_B and GluL212
hydroxyls placed	dynamically	ground state	ground state		ground state	not reported
ΔG_{AB} (pH 7)	−80 meV	not reported	+165 meV		not reported	−160 meV

[a] Ionization states of residues in the cluster in the ground state at pH = 7.

uptake from solution but rather a proton shift between GluL212 and AspL213.

Each of the acids in the cluster has several possible neutral and ionized positions (Figure 1a). The neutral form of GluL212 is distributed over three rotamers with similar occupancy. The ratio of these conformers is not a function of pH. When GluL212 begins to become ionized, two different rotamers are populated. Two ionized and one neutral conformer of AspL213 and three ionized and one neutral conformer of AspL210 are significantly populated (Figure 7a). The predominant conformer of AspL213 is in a position to make a good hydrogen bond to SerL223.

Reduction of Q_A causes only small changes in proton distribution within the cluster (Figure 7b), with the net charge of these three residues remaining the same as in the ground state at any pH. However, these small changes 15 Å away from Q_A are among the largest that occur on Q_A reduction. In contrast, when the electron is transferred from Q_A^- to Q_B at pH 7−8, there is significant rearrangement of both the atomic positions and charges in this cluster. AspL213 binds a proton, breaking the hydrogen bond to SerL223 which now makes a hydrogen bond to Q_B^-. AspL213 and AspL212 have one proton in the ground state or in the Q_A^- state. However, in the Q_B^- state both acids are fully protonated (Figures 7c). Thus, on electron transfer from Q_A^- the cluster goes from a charge of −1 with $[Q_B^0 + (L212{:}L213)^{-1} + L210^0]$ to a charge of −2 with $[Q_B^{-1} + (L212{:}L213)^0 + L210^{-1}]$ (Table 2).

GluL212, AspL213, and AspL210 form a inner cluster near Q_B which is surrounded by many other acids and bases. GluL212:AspL213 have one charge and one proton in the ground state while both acids are protonated in the Q_B^- state. So over the entire pH range studied here, a proton must be bound by L212:L213 on Q_B reduction. Between pH 7 and pH 9 this is accomplished by an intracluster proton shift as most of this proton is donated by AspL210. Figure 5 describes the proton uptake on electron transfer from Q_A^- to Q_B, comparing the role of AspL210, AspL213, the rest of the protein, and the solvent. At pH 8 L213 binds 0.95 H^+/RC and L210 releases 0.75 H^+/RC. Of the extra 0.20 H^+/RC bound by L213, 0.15 is transferred from other sites in the protein, each contributing <0.03 H^+/RC, while only 0.05 is donated from solution. The residues surrounding the cluster thus add to the buffer capacity, ensuring that the net proton uptake into the protein is smaller than the increase in the cluster's protonation (Figure 5). Proton shifts from surrounding residues play a larger role at higher and lower pH's. Below pH 6 L210 holds onto its proton in the Q_B^- state so protonation of L213 requires transfer from the protein and the solvent. Above pH 9 L210 is largely ionized in both ground and Q_B^- states so again proton import into the cluster must occur.

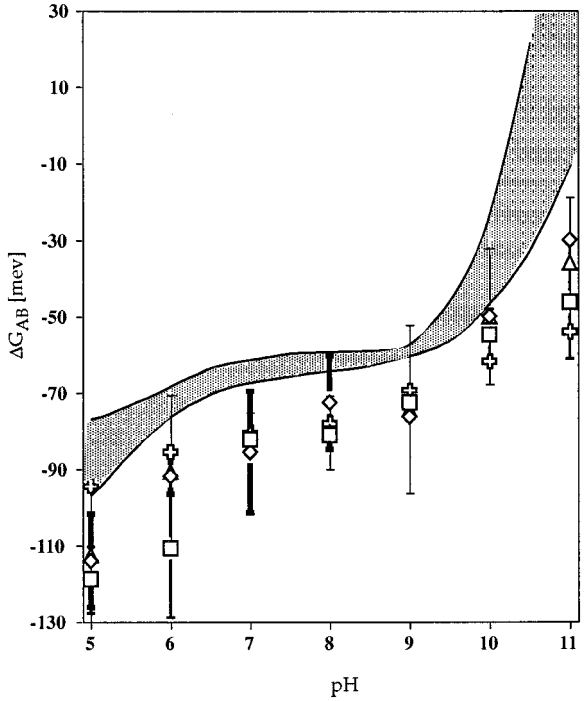

FIGURE 8: Free energy of Q_A^- to Q_B electron transfer calculated by method 1 (▲) (neutral P), method 2 [neutral P (□) and oxided P (◇)], and method 3 (✣) (neutral P). Experimental data taken from refs 32, 33, and 101 outline the shadowed region. Error bars: method 1, thick lines; method 2, thin light lines.

Free Energy of Electron Transfer. The free energy of Q_A^- to Q_B electron transfer (ΔG_{AB}) was calculated by the three methods described in the Methods section and compared with the experimentally measured value for this reaction from pH 5 to pH 11 (Figure 8). There is good agreement between experiment and calculation over the entire pH range. At pH 7 the measured ΔG_{AB} is −65 meV while the calculated value is −80 ± 10 meV (method 1) and −82 ± 6 meV (method 2). The reaction becomes more favorable below pH 6 and less favorable at pH 9 and above in both experiment and calculation.

Dependence of ΔG_{AB} on the Conformational Flexibility of the Protein. Previous calculations have been made of the coupling between electron and proton transfer for the electron transfer from Q_A^- to Q_B (*19*−*21*, *42*). These studies assumed a rigid protein where only the charge on acids and bases

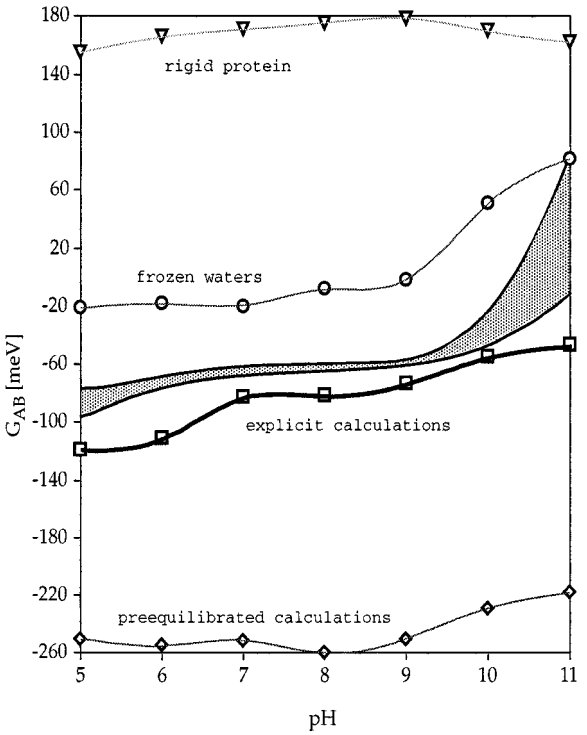

FIGURE 9: Free energy of Q_A^- to Q_B electron transfer calculated with different degrees of conformational flexibility. Rigid protein: the protein structure and waters are rigid; only changes in ionization state are allowed. Frozen waters: protein has conformational degrees of freedom, but waters are kept frozen. Explicit calculations: protein and waters are flexible. Preequilibrated calculations: energy is estimated in proteins that are equilibrated in the Q_A^- and Q_B^- states (see Results for more details). The range of experimental data is shown by the shadowed region.

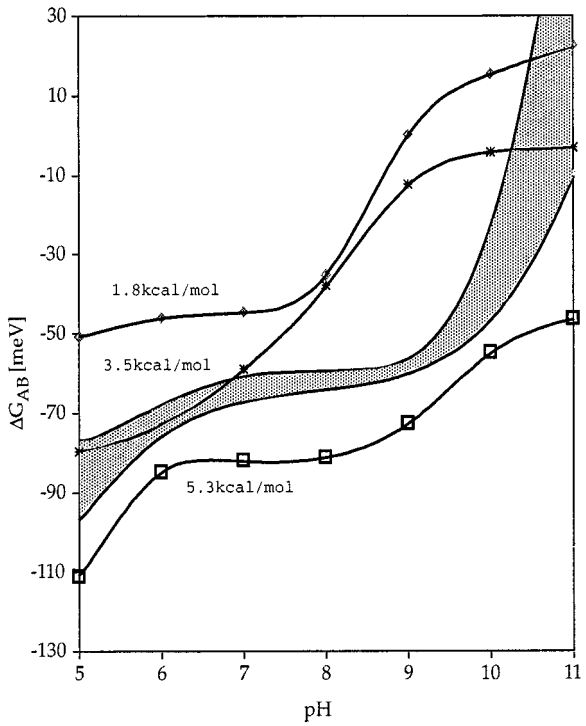

FIGURE 10: Free energy of Q_A^- to Q_B electron transfer calculated by method 2 with different energies to transfer a water from bulk solution into the protein. Experimental data are shown as the shadowed region.

could change. The MCCE method allows the protein to sample many additional atomic positions in addition to the changes in ionization state. The free energy for electron transfer was determined in a rigid structure to estimate the impact of the added flexibility. This requires selecting one atomic conformation for each residue. The residue conformer with the highest occupancy in an MCCE calculation in the ground state at pH 7 was chosen. Waters were deleted and DelPhi calculations were carried out with a high dielectric constant in the cavities. These conditions reproduce those used in earlier methods. ΔG_{AB} was determined from the ratio of Q_A^- and Q_B^- in accepted microstates (method 2) (Figure 9).

In a protein where atomic positions are fixed and acid and base protonation states can change, the reaction is uphill by 160 meV rather than downhill by −65 meV, in agreement with previous calculations (*19*) (Figure 9). In fact, the reaction is so unfavorable that there is an insufficient population of Q_B^- in the Monte Carlo simulation to accurately determine the population ratio. This state was artificially made more favorable by −2.36 kcal/mol, and then the results were corrected using the method of Beroza et al. (*19*). Thus, atomic rearrangement, in particular of SerL223 (100 meV) and AsnM44 (20 meV), is required to stabilize the Q_B^- state. ΔG_{AB} was also calculated, allowing protein flexibility but using explicit but rigid waters (Figure 9). In the flexible protein with frozen waters ΔG_{AB} is about 160−180 meV more favorable than in the rigid protein. The free energy with frozen and mobile waters differs by about 60 meV. Small motions of many waters are responsible for this difference.

The free energy of moving the electron from Q_A^- to Q_B can be estimated in proteins that are equilibrated in the Q_A^- state and the Q_B^- state. The average energy of putting the electron on the Q_A^- ensemble is (the potential at Q_A) × (the charge on Q_A^-) + (the reaction field energy of Q_A^-). A similar calculation can be performed for Q_B^-, collecting potentials at Q_B in a protein where all microstates have Q_B^-. The difference between these two energies is −260 meV, 180 meV more favorable than ΔG_{AB}. The unfavorable energy difference comes from the intraprotein energy terms for the ensemble of microstates with Q_A^- and those with Q_B^-. Thus, the cost of rearranging the protein to stabilize Q_B^- is 180 meV.

Sensitivity of the Calculation to the Water Transfer Energy. The calculations assume a penalty for transferring water molecules out of bulk solution into the protein. If there is insufficient energy of interaction with the protein, no waters will be found in the site; rather a water conformation that does not interact with the protein will be populated. The calculations discussed above use a transfer energy of 5.3 kcal/mol (*66*). Calculations were also performed with transfer energies of 1.7 and 3.5 kcal/mol. With a penalty of only 1.7 kcal/mol 122 waters remain in the protein. Thus, 97% of the sites are occupied. With a transfer energy of 3.5 kcal/mol there are 104 waters (83% site occupancy) while with 5.3 kcal/mol only 62 waters are found (49% site occupancy).

The free energy of electron transfer from Q_A^- to Q_B was calculated with the different water transfer penalties (Figure 10). The value at pH 7.0 is weakly dependent on the number of waters in the protein, changing from −50 to −80 meV as the transfer energy is increased. However, the pH dependence

of ΔG_{AB} is strongly dependent on the treatment of waters. On the reduction of Q_B there is a loss in water site occupancy in water 6 and in water channels near Q_B. As the transfer penalty is reduced, these waters cannot leave the protein, resulting in the observed shifts in the pH dependence of ΔG_{AB}.

DISCUSSION

The electron transfer from Q_A^- to Q_B in bacterial RCs has been the subject of several earlier theoretical studies considering both *Rb. sphaeroides* (*19*, *42*) and *Rps. viridis* RCs (*20*, *21*). In some respects all calculations provide a similar picture. All found that at physiological pH's all basic groups (except His) are fully ionized and do not undergo ionization changes upon quinone reduction (*18*−*21*, *42*). Again there is agreement that most Asp's and Glu's are ionized. As many of these residues are deeply buried in the protein, all of the electrostatic calculations on RCs show that these proteins are designed to stabilize buried charges.

Each calculation has found a cluster of acids in the Q_B site that is not fully ionized (Table 2). Redistribution of protons within the cluster and uptake of protons into the cluster from the rest of the protein or solvent occur when Q_B is reduced. Residues GluL212, AspL213, and AspL210 interact strongly with each other and with Q_B in *Rb. sphaeroides* RCs (*19*, *42*). These residues have also been recognized as important by site-directed mutagenesis studies (*34*, *36*, *83*−*85*). In *Rps. viridis* L213 is an Asn not an Asp so the groups that make up the cluster must be different. The glutamic acids L212, H177 (H173 in *Rb. sphaeroides*), and M234 are now identified as the active cluster (*20*, *21*). In the ground state at physiological pH each calculation finds a net charge of −1 (here) to −2 distributed among the three acids. This provides one to two protons in the cluster that can change position when Q_B is reduced, diminishing the requirement for proton uptake from solution to stabilize the quinone charge.

In both *Rb. sphaerodies* and *Rps. viridis* RCs the cluster is embedded in a large group of strongly interacting acids and bases. In *Rps. viridis* 24 residues can be connected to Q_B by a chain of interactions of more than 2 ΔpK units (2.7 kcal/mol). This web extends over 25 Å (*20*). Similar connectivity can also be found in *Rb. sphaeroides* RCs (*15*, *19*). In addition, a very positive potential created by the backbone dipoles plays a role in allowing buried acids near Q_B to remain ionized (*19*, *20*, *86*). The extended web plays an important role through electrostatic interactions that help to determine the protonation equilibrium within the active cluster. However, the cluster is special. First, strong, mutually unfavorable interactions inhibit all three acids from being ionized simultaneously. Second, if each acid were to be analyzed in the absence of the other members of the cluster but in the presence of the rest of the protein, similar pK_a's would be calculated for each. It is the latter requirement that makes it difficult to identify the active cluster simply by inspection of the structure. When these two conditions are met, there are small free energy differences between microstates with a proton on any particular member of the cluster. These interactions often yield ensembles of RCs with different proton distributions. Microstates with each of these charge distributions must be close in energy. This is why the precise distribution of the proton over the three acids is difficult to establish (Table 2). The ionization of Q_B then shifts the balance of ionization states in the cluster.

The partial protonation of several sites means that the population of RCs will be heterogeneous at equilibrium. A number of reports have been made of heterogeneous rates of electron transfer from Q_A^- to Q_B in chromatophores (*40*) and isolated RCs (*41*, *87*). If the redistribution of protonation states is slow on the time scale of intra-RC reactions, the heterogeneity of protonation states could contribute to the observed heterogeneity of the reaction rate.

A cluster of strongly interacting acids has also been found in other integral membrane proteins that transport charge across the membrane (*88*, *89*). Calculations on bacteriorhodopsin identify Asp212 and Asp85 as a pair of coupled residues with complicated titration behavior (*90*−*92*). In cytochrome *c* oxidase a cluster of 18 titratable groups controls most of the proton uptake associated with redox changes at the binuclear site (*7*). Thus, clusters may be a common feature allowing intraprotein proton transfer in response to changes in ionization of deeply buried cofactors (*20*). Clusters can reduce the need for rapid proton transfer from solution to stabilize the reaction at these cofactors. By redistribution of protons the cluster serves to stabilize both product and reactant cofactor ionization states, providing a local, designed, region that increases the effective dielectric response of the protein to the reaction.

Free Energy of the Electron-Transfer Reaction. All previous calculations in *Rb. sphaeroides* RCs either did not report the free energy of electron transfer from Q_A^- to Q_B (ΔG_{AB}) (*42*) or provided a free energy that was very unfavorable (*19*) (see Table 2). The calculations of Beroza et al. (*19*) used standard methodology for pK_a calculations (*67*, *93*). Waters were removed, hydroxyl protons were minimized in the protein ground state, and only ionization states of acidic and basic residues change when the redox state of the protein changes. The earlier calculations provided a ΔG_{AB} of +165 meV. This is the same as the value obtained here under the same conditions (Figure 9). It is probably fortuitous that these values for ΔG_{AB} are numerically so close since different crystal structures, charge sets, and hydroxyl positions were used. However, both studies show that without conformational flexibility electron transfer from Q_A^- to Q_B is unfavorable.

Calculations on *Rps. viridis* RCs have also found the electron transfer from Q_A^- to Q_B to be unfavorable in a rigid protein (R. Lancaster and M. R. Gunner, unpublished). However, the rigid protein calculations of Rabenstein et al. (*21*) do reproduce the measured ΔG_{AB} at pH 7, the pH of their calculations. Several specific changes in the structure were made. Q_B was moved and the side chain of GluL212 was rotated to incorporate findings from a new, at the time unpublished *Rps. viridis* structure (*94*). New distributions of charges on ionized and neutral quinones were used. With these charges the interaction of Q_B^- with GluL212 is 100 meV less unfavorable. This will not affect ΔG_{AB} because L212 is neutral in all charge states of the protein here as well as in their *Rps. viridis* structure calculation. Changes in the pairwise electrostatic interactions of 25−40 meV were found between Q_B^- and particular conformers of GluH173, GluM323, and GluM234; ArgL213 and ArgL217; and SerL223. Only half of these changes stabilize Q_B^-, so it is

not possible to simply determine what the resulting effect would be. Future calculations will be needed to test the sensitivity of the outcome to the charge distribution.

The free energy of the electron transfer from Q_A^- to Q_B was calculated with three different levels of flexibility: at pH 7 in a standard rigid protein calculation ΔG_{AB} was +170 meV; when the protein side chains can move, but the waters were fixed in their ground state orientation, $\Delta G_{AB} = -20$ meV while in the full MCCE simulation ΔG_{AB} was −80 meV. Thus, conformational flexibility must be coupled to the ionization changes to create the favorable reaction free energy. The changes in conformation and ionization on reduction of Q_B show that work goes into the protein to create the favorable environment for Q_B^-. The energy of interaction of Q_B^- with the protein during Monte Carlo sampling of equilibrium microstates with Q_B^- is 260 meV more favorable than the interaction of Q_A^- with the protein when the simulation contains only Q_A^-. However, ΔG_{AB} is only −80 meV. Thus, if the interaction with the quinone is removed, the distribution of protein conformations formed with Q_B^- is 180 meV less favorable than with Q_A^-. The less favorable intraprotein interactions but more favorable protein−quinone interactions in the Q_B^- state yield the final observed free energy. This balance of interaction energies is found whenever conformation changes are used to stabilize a charge. Such a response can be described as dielectric relaxation around the new charge.

The requirement for conformational flexibility found in the calculation is in agreement with the experimental observation that the electron transfer from Q_A^- to Q_B will not occur in samples frozen in the ground state. However, if the samples are trapped in the $P^+Q_B^-$ state, by freezing under illumination, the electron transfer can occur (*95*). It is not known whether the required changes include the movement of the Q_B itself from the distal to the proximal position (*17*) or if any of the changes in heavy atom positions discussed here contribute. In these calculations the electron transfer from Q_A^- would never be favorable to the distal Q_B position. However, even if the quinone was in the inner site, the reaction is uphill without the changes in conformation and protonation of the groups in the cluster.

How the Protein Stabilizes the Charges on the Cofactors. Processes that bury charges in proteins are energetically costly because of the desolvation of the charge. Introducing charges into proteins has been shown to often be unfavorable. For example, protein stability can decrease when a charge is added by site-directed mutation (*96*, *97*). However, in the heterogeneous protein environment the new charge may be stabilized in a number of ways (*6*): (1) The uptake of protons and electrons can occur simultaneously to maintain electroneutrality of the electron-transfer process. (2) A static nonzero potential in the appropriate locations can be generated by the structure (*6*, *18*). This design may destabilize the ground state of the protein but will stabilize the buried charge. (3) Internal charges and dipoles can rearrange when a charge binds, creating a dielectric response which stabilizes the charge.

In the electron transfers from P, the sequential electron acceptors H_L and Q_A are each at a more positive electrostatic potential than the electron donor stabilizing the charge-separated state (*18*) without proton uptake or protein rearrangement. These reactions will occur in frozen samples (*95*). In contrast, electron transfer from Q_A^- to Q_B will not occur without protein rearrangement, so the difference in static potential at Q_A and Q_B is not sufficient to favor electron transfer. There is little additional proton uptake as the electron is passed from Q_A^- to Q_B. However, there is significant rearrangement of the protein which stabilizes the charge. Thus the reaction mechanism uses protein rearrangement rather than proton binding or a preexisting static field to stabilize the charge on Q_B.

At physiological pH's, Q_A reduction causes small ionization changes (Figures 2 and 3a,b) of acidic groups in the Q_B pocket, which are more than 15 Å away, while the region of the protein near Q_A does not undergo any large ionization or conformation changes (Figures 2 and 3a,b). This is consistent with the experimental observation that mutations in the Q_B pocket affect the behavior of the Q_A^- state (*98*). The pattern of small changes dispersed throughout the protein shows the Q_A site to have some of the characteristics of a medium with a low effective dielectric constant.

In contrast, Q_B reduction causes large changes in ionization states and hydroxyl, side-chain, and water conformations near Q_B (Figures 2 and 3c,d). Thus, Q_B looks like an environment with a relatively high effective dielectric constant. Local rearrangements screen more distant sites from the effects of a new charge, and these rearrangements stabilize the charge so no additional proton uptake is required.

Proton Uptake Coupled to Electron Transfer and Role of Specific Residues near Q_B. The small pH dependence of the ΔG_{AB} for electron transfer from Q_A^- to Q_B between pH 7 and pH 10 in *Rps. viridis* (*99*, *100*) and between pH 6 and pH 9 in *Rb. sphaeroides* RCs (*32*, *101*, *102*) is the experimental signature of a reaction where the proton uptake is close to zero (eq 8). A group of ionized bases (ArgL217, LysH130, and several others), acidic groups (AspL210, L213, GluL212, H173), hydroxyl groups (SerL223, TyrM222), AsnM44, and nearby buried waters play key roles in stabilizing Q_B^-. Some, such as the bases and GluH173, do not change their ionization states upon Q_B reduction, but they strongly influence the electrostatic potential at the other residues. Others, such as L210 and L213, change their ionization or conformation actively modifying ΔG_{AB}.

The calculations reported here duplicate the experimentally determined pH dependence of ΔG_{AB} from pH 5 to pH 11. In the physiological pH range the acid cluster of L210, L212, and L213 plus SerL223 plays a pivotal role. GluL212 and AspL213 are practically symmetrically situated around Q_B and so interact with the quinone by almost the same amount (Figure 6). However, AspL213 interacts with AspL210 more strongly than with GluL212. Thus, AspL213 can control the ionization of AspL210 while GluL212 is less effective. In the ground state and the Q_A^- state there is one proton on L212 and L213. If the ionized acid is L213, then L210 is also protonated. When Q_B is reduced, L212 and L213 must both be protonated. If possible, the proton comes in from L210, 10 Å away from Q_B. However, if L210 is ionized in the Q_A^- state, L213 is protonated by transfer from the rest of the protein and solution. L210 is ionized in the Q_A^- state at higher pH, and so significant proton uptake is seen. In addition, L210 will be ionized if L213 is neutral in response to L212 ionization. Solution proton uptake will now be more coupled to Q_B reduction and ΔG_{AB} will become pH dependent. This may account for the larger pH dependence of ΔG_{AB}

found in earlier calculations where L212 and L210 are partially ionized in the ground state (Table 2) (*19*).

The roles of the residues in the cluster are in agreement with the picture obtained by site-directed mutagenesis experiments which suggest that AspL213 and SerL223 are involved in the first proton transfer to Q_B (*20*, *34*, *35*, *42*, *83*) which occurs following a second electron transfer to generate $Q_A^-Q_B^-$. The calculations (Figure 1b) find this chain of residues moving into a configuration that can deliver the proton to Q_B^-. The proton is transferred from AspL210 to AspL213 when Q_B^- is formed. This proton transfer breaks the hydrogen bond between AspL213$^-$ and SerL223, reorienting the Ser hydroxyl to make a hydrogen bond to Q_B^-. L223 is then properly situated and L213 is protonated and prepared for proton transfer to Q_B^-. Such a scenario was also suggested on the basis of the RC structure (*94*). The proton transfer to Q_B^- is energetically unfavorable, but it appears to precede the second reduction of Q_B (*103*). Final reduction of Q_B to dehydroquinone does require proton binding from solution. Several water channels can be identified near Q_B and Q_A that could transfer protons inward. There are breaks in each channel given waters from only one structure. However, combining waters from all four structures yields better connectivity of the hydrogen bond network within the channels.

Comparison with the Results from Site-Directed Mutations. The free energy of proton uptake has been measured for many mutants to access their effect on the different stages of Q_B reduction including the first electron-transfer reaction described here. Full analysis of these mutants has not yet been carried out. However, it is possible to simply consider how mutations of cluster residues may change RC function in light of the picture of their role presented here.

In the GluL212 to Gln mutant the first electron transfer to Q_B remains essentially unimpaired (*84*, *104*). Until pH 10 the behavior is identical to that of the wild-type RCs; however, there is no increase in proton uptake and accompanying less favorable ΔG_{AB} at high pH. It has been suggested that L212 is neutral in the ground state so its removal does not influence the reaction (pH <10). Its ionization at higher pH's would then yield the observed change in ΔG_{AB}. The calculations reported here do find that GluL212 is protonated at physiological pH's and so has an unusually high pK_a. However, in the presence of L213$^-$, GluL212 remains neutral beyond pH 11 (Figure 7). The proton uptake and changes in ΔG_{AB} above pH 9 are largely a result of the inability of L210 to be protonated in the ground state so that much of the proton transfer into L213 now comes from solution.

In the AspL213 to Asn mutant ΔG_{AB} favors reduced Q_B by -140 meV rather than the -65 meV found in the wild-type protein (*34*, *83*). This observation is consistent with our finding that AspL213 is the residue that changes its protonation state on Q_B reduction. If the conformer of L213 that makes a hydrogen bond to SerL223 is forbidden, Q_B^- is stabilized relative to Q_A^- by an amount comparable to that found in the L213 mutation (data not shown). In these RCs L213 is neutral and L212 ionized in the ground and Q_A^- states. L212 now binds a proton on ionization of Q_B. The electrostatic environment of both quinones is similar to that found for the wild-type protein. The change in ΔG_{AB} is not due to a stabilization of the Q_B^- state but to the loss of the hydrogen bond between L213 and L223, destabilizing the protein in the Q_A^- state.

In calculations reported here AspL210 has a strong impact on the pH dependence of the reaction. ΔG_{AB} is pH dependent below the pK_a of AspL210 in the ground state at 6.8 and above its pK_a at 9.5 in the Q_B^- state. In the AspL210 to Asn mutant the high pH transition is shifted from pH 9 to pH 7 (*85*). The reaction is pH independent, with a ΔG_{AB} which favors Q_B^- slightly more than the wild type from pH 4 to pH 7. The large shifts in the regions of pH dependence support a role for L210 in the pH dependence of ΔG_{AB}. The broad pH-independent region at lower pH suggests that another residue may substitute, forming another cluster that can transfer protons into L212:L213 as Q_B is reduced.

When SerL223 is replaced with an Ala, ΔG_{AB} favors Q_B^- by a small amount (*35*). The change in ΔG_{AB} is much smaller than found for deletion of L213. This could indicate that the strength of the hydrogen bond to L213 stabilizing the Q_A^- states is comparable to that of the hydrogen bond to Q_B^- so the loss of Ser destabilizes reactant and product by a similar amount. Alternatively, other groups such as a water may substitute for the Ser OH (*35*).

Comparison with the Results of Infrared Spectroscopy. Infrared spectroscopy can provide direct information about the residues involved in the Q_A^- to Q_B electron transfer (*105*−*110*). There is one IR band that changes on reduction of Q_B in the region identified with the carboxylic group of amino acids. This band is missing in the GluL212 to Gln mutant (*107*) but is present in the AspL213 to Asn, AspL210 to Asn, and GluH173 to Gln mutants (*105*, *110*, *111*). Thus, it appears that GluL212 should be partially ionized in the ground state at pH 7 and should be protonated in the Q_B^- state. This has also been suggested by previous calculations (*19*, *42*). In contrast, here L212 is protonated at physiological pH's and so cannot bind a proton on Q_B reduction. The identification of the IR band with GluL212 seems firm as it is absent only in the L212 mutant while it is seen in the difference spectrum of other mutants (*105*, *110*, *111*). In addition, the spectral shift is demonstrated to be proton uptake rather than an electrochemical response to Q_B reduction since it has the appropriate shift when protons are replaced with deuterons. Thus, the role of GluL212 seen in the FTIR measurements and in the calculations represents the most significant disagreement of the MCCE calculations with experiment.

Are the Changes in the Protein That Occur on Electron Transfer Unique? The results presented here provide calculated values for ΔG_{AB} and for proton uptake as four different redox states of the protein are formed that agree quite well with the experimental data. Motions and changes in charge state throughout the protein are found. Underlying these results is a cluster of residues near Q_B that are active participants in the electron transfer from Q_A^- to Q_B. This model with the cluster playing a central role in the physiological range can certainly account for many measurements. However, the IR data appear to provide a different role for GluL212. It is too early to tell if the model presented here is the only way to get the observed results. Thus, it may be that alternate conformers that are not present or are inaccessible maintaining the backbone of the 1aij structure could also reproduce experimental data utilizing different groups of residues. The ability of various second site revertants to

recover near wild-type behavior shows that this cluster can be replaced (*28*). In addition, *Rps. viridis* and *Rb. sphaeroides* RCs have very similar behavior with two different clusters of residues. Future calculations comparing RCs from different bacteria or with different mutations may give us additional insign into the flexibility and robustness of these proteins.

ACKNOWLEDGMENT

We thank George Feher and Ed Abresh for access to the 1aij and 1aig structures prior to their deposition in the Protein Data Bank and Jacques Breton, Eliane Nabedryk, Pierre Sebban, Colin Wraight, Mel Okamura, Mark Paddock, and Boris Atanasov for helpful discussions.

REFERENCES

1. Russell, S. T., and Warshel, A. (1985) *J. Mol. Biol. 185*, 389−404.
2. Warshel, A., and Åqvist, J. (1991) *Annu. Rev. Biophys. Chem. 20*, 267−298.
3. Warshel, A., and Papazyan, A. (1998) *Curr. Opin. Struct. Biol. 8*, 211−217.
4. Honig, B., and Nicholls, A. (1995) *Science 268*, 1144−1149.
5. Honig, B. (1993) *Curr. Opin. Struct. Biol. 3*, 223−224.
6. Gunner, M. R., Alexov, E., Torres, E., and Lipovaca, S. (1997) *J. Biol. Inorg. Chem. 2*, 126−134.
7. Kannt, A., Roy, C., Lancaster, D., and Michel, H. (1998) *Biophys. J. 74*, 708−721.
8. Noji, H., Yasuda, R., Yoshida, M., and Kinosita, K. (1997) *Nature 386*, 299−302.
9. Brown, L. S., Kamikubo, H., Zimanyi, L., Kataoka, M., Tokunaga, F., Verdegem, P., Luntenburg, J., and Lanyi, J. K. (1997) *Proc. Natl. Acad. Sci. U.S.A. 94*, 5040−5044.
10. Zimanyi, L., Cao, Y., Needleman, R., Ottolenghi, M., and Lanyi, J. K. (1993) *Biochemistry 32*, 7669−7678.
11. Blankenship, R. E., Madigan, M. T., and Bauer, C. E. (1995) *Anoxygenic Photosynthetic Bacteria*, Vol. 2, Kluwer Academic Publishers, Dordrecht, The Netherlands.
12. Gunner, M. R. (1991) *Curr. Top. Bioenerg. 16*, 319−367.
13. Okamura, M. Y., and Feher, G. (1995) in *Advances in Photosynthesis* (Blankenship, R., Madigan, M., and Bauer, C., Eds.) pp 577−593, Kluwer Academic Publishers, Dordrecht, The Netherlands.
14. Deisenhofer, J., Epp, O., Miki, R., and Michel, H. (1985) *Nature 318*, 618−624.
15. Ermler, U., Fritzsch, G., Buchanan, S. K., and Michel, H. (1994) *Structure 2*, 925−936.
16. Deisenhofer, J., and Michel, H. (1989) *EMBO J. 8*, 2149−2170.
17. Stowell, M. H. B., McPhillips, T. M., Rees, D. C., Soltis, S. M., Abresch, E., and Feher, G. (1997) *Science 276*, 812−816.
18. Gunner, M. R., Nicholls, A., and Honig, B. (1996) *J. Phys. Chem. 100*, 4277−4291.
19. Beroza, P., Fredkin, D. R., Okamura, M. Y., and Feher, R. (1995) *Biophys. J. 68*, 2233−2250.
20. Lancaster, C. R. D., Michel, H., Honig, B., and Gunner, M. R. (1996) *Biophys. J. 70*, 2469−2492.
21. Rabenstein, B., Ullmann, G. M., and Knapp, E.-W. (1998) *Biochemistry 37*, 2488−2495.
22. Beroza, P., and Case, D. (1996) *J. Phys. Chem. 100*, 20156−20163.
23. Alexov, E. G., and Gunner, M. R. (1997) *Biophys. J. 72*, 2075−2093.
24. Okamura, M. Y., and Feher, G. (1992) *Annu. Rev. Biochem. 61*, 861−896.
25. Takahashi, E., and Wraight, C. A. (1994) *Adv. Mol. Cell Biol. 10*, 197−251.
26. Hanson, D. K., Baciou, L., Tiede, D. M., Nance, M., Schiffer, M., and Sebban, P. (1992) *Biochim. Biophys. Acta 1102*, 260−265.
27. Rongey, S. H., Paddock, M. L., Feher, G., and Okamura, M. Y. (1993) *Proc. Natl. Acad. Sci. U.S.A. 90*, 1325−1329.
28. Hanson, D. K., Tiede, D. M., Nance, S. L., Chang, C., and Schiffer, M. (1993) *Proc. Natl. Acad. Sci. U.S.A. 90*, 8929−8933.
29. Sebban, P., Maroti, P., Schiffer, M., and Hanson, D. K. (1995) *Biochemistry 34*, 8390−8397.
30. Maroti, P., Hanson, D. K., Schiffer, M., and Sebban, P. (1995) *Nature Struct. Biol. 2*, 1057−1059.
31. Maroti, P., and Wraight, C. A. (1997) *Biophys. J. 73*, 367−381.
32. McPherson, P. H., Okamura, M. Y., and Feher, G. (1988) *Biochim. Biophys. Acta 934*, 348−368.
33. Maroti, P., and Wraight, C. A. (1988) *Biochim. Biophys. Acta 934*, 329−347.
34. Paddock, M. L., Rongey, S. H., McPherson, P. H., Juth, A., Feher, G., and Okamura, M. Y. (1994) *Biochemistry 33*, 734−745.
35. Paddock, M. L., Feher, G., and Okamura, M. Y. (1995) *Biochemistry 34*, 15742−15750.
36. Paddock, M. L., Feher, G., and Okamura, M. Y. (1997) *Biochemistry 36*, 14238−14249.
37. Baciou, L., and Michel, H. (1995) *Biochemistry 34*, 7967−7972.
38. Valerio-Lepiniec, M., Delcroix, J. D., Schiffer, M., Hanson, D., and Sebban, P. (1997) *FEBS Lett. 407*, 159−163.
39. Abresch, E. C., Paddock, M. L., Stowell, M. H. B., McPhillips, T. M., Axelrod, H. L., Soltis, S. M., Rees, D. C., Okamura, M. Y., and Feher, G. (1998) *Photosynth. Res. 55*, 119−125.
40. Tiede, D. M., Vazquez, J., Cordova, J., and Marone, A. P. (1996) *Biochemistry 35*, 10763−10775.
41. Li, J., Gilroy, D., Tiede, D. M., and Gunner, M. R. (1998) *Biochemistry 37*, 2818−2829.
42. Gunner, M. R., and Honig, B. (1992) in *The Photosynthetic Bacterial Reaction Center: Structure, Spectroscopy and Dynamics II* (Breton, J., and Vermeglio, A., Eds.) pp 403−410, Plenum, New York.
43. Sham, Y. Y., Muegge, I., and Warshel, A. (1998) *Biophys. J. 74*.
44. Nakamura, H. (1996) *Q. Rev. Biophys. 29*, 1−90.
45. Ripoll, D. R., Vorobjev, Y. N., Liwo, A., Vila, J. A., and Scheraga, H. A. (1996) *J. Mol. Biol. 264*, 770−783.
46. You, T. J., and Bashford, D. (1995) *Biophys. J. 69*, 1721−1733.
47. Zhou, H., and Vijayakumar, M. (1997) *J. Mol. Biol. 267*, 1002−1011.
48. Vlijmen, H. W. T., Schaefer, M., and Karplus, M. (1998) *Proteins 33*, 145−158.
49. Berstein, F. C., Koetzle, T. F., Williams, G. J. B., Meyers, E. F. J., Brice, M. D., Rodgers, J. R., Kennard, O., Shimanouchi, T., and Tasumi, M. (1977) *J. Mol. Biol. 112*, 535−542.
50. Chang, C.-H., El-Kabbani, O., Tiede, D., Norris, J., and Schiffer, M. (1991) *Biochemistry 30*, 5352−5360.
51. Komiya, H., Yeates, T. O., Rees, D. C., Allen, J. P., and Feher, G. (1988) *Proc. Natl. Acad. Sci. U.S.A. 85*, 9012−9016.
52. Hooft, R. W. W., Sander, C., and Vriend, G. (1996) *Proteins 26*, 363−376.
53. Bharadwaj, R., Windemuth, A., Sridharan, S., Honig, B., and Nicholls, A. (1995) *J. Comput. Chem. 16*, 898−913.
54. Nicholls, A., and Honig, B. (1991) *J. Comput. Chem. 12*, 435−445.
55. Sitkoff, D., Sharp, K. A., and Honig, B. (1994) *J. Phys. Chem. 98*, 1978−1988.
56. Parson, W. W., Chu, Z.-T., and Warshel, A. (1990) *Biochim. Biophys. Acta 1017*, 251−272.
57. Gilson, M. K., and Honig, B. (1988) *Proteins 4*, 7−18.
58. Gu, Z., Riendenour, C. F., Bronnimann, C. E., Iwashita, T., and McDermott, A. (1996) *J. Am. Chem. Soc. 118*, 822−829.
59. Kossiakoff, A. A., Shpungin, J., and Sintchak, M. D. (1990) *Proc. Natl. Acad. Sci. U.S.A. 87*, 4468−4472.
60. McDowell, R., and Kossiakoff, A. (1995) *J. Mol. Biol. 250*, 553−570.
61. Kossiakoff, A. A., Ultsch, M., White, S., and Eigenbrot, C. (1991) *Biochemistry 30*, 1211−1221.
62. Dunbrack, R. L., and Cohen, F. E. (1997) *Protein Sci. 6*, 1661−1681.

63. Jeffrey, G. A., and Saenger, W. (1991) *Hydrogen Bonding in Biological Structures*, Springer-Verlag, Berlin.
64. Brunger, A. T., and Karplus, M. (1988) *Proteins 4*, 148−156.
65. Sitkoff, D., Sharp, K. A., and Honig, B. (1994) *Biophys. Chem. 51*, 397−409.
66. Wolfenden, R., and Radzicka, A. (1994) *Science 265*, 936−937.
67. Yang, A.-S., Gunner, M. R., Sampogna, R., Sharp, K., and Honig, B. (1993) *Proteins 15*, 252−265.
68. Niimura, N., Minezaki, Y., Nonaka, T., Castagna, J.-C., Cipriani, F., Hoghoj, P., Lehmann, M. S., and Wilkinson, C. (1997) *Nature Struct. Biol. 4*, 909−914.
69. Gilson, M. K., and Honig, B. H. (1986) *Biopolymers 25*, 2097−2119.
70. Antosiewicz, J., McCammon, J. A., and Gilson, M. K. (1996) *Biochemistry 35*, 7819.
71. Antosiewicz, J., McCammon, J. A., and Gilson, M. K. (1994) *J. Mol. Biol. 238*, 415−436.
72. Antosiewicz, J., Briggs, J. M., Elcock, A. H., Gilson, M. K., and McCammon, J. A. (1996) *J. Comput. Chem. 14*, 1633−1644.
73. Oberoi, H., and Allewell, N. (1993) *Biophys. J. 65*, 48−55.
74. Simonson, T., Perahia, D., and Brunger, A. T. (1991) *Biophys. J. 59*, 670−690.
75. Simonson, T., and Perahia, D. (1995) *Comput. Phys. Commun. 1995*, 291−303.
76. Simonson, T., and Perahia, D. (1995) *J. Am. Chem. Soc. 117*, 7987−8000.
77. Sharp, A. S. (1998) *Biophys. J. 73*, 1241−1250.
78. Schellman, J. A. (1975) *Biopolymers 14*, 999−1018.
79. Gilson, M. K., Given, J. A., and Head, M. S. (1997) *Chem. Biol. 4*, 87−92.
80. Chang, C. H., Tiede, D., Tang, J., Smith, U., Norris, J., and Schiffer, M. (1986) *FEBS Lett. 205*, 82−86.
81. Williams, J. C., Steiner, L. A., and Feher, G. (1986) *Proteins 1*, 312−325.
82. Alden, R. G., Parson, W. W., Chu, Z. T., and Warshel, A. (1996) *J. Phys. Chem. 100*, 16761−16770.
83. Takahashi, E., and Wraight, C. A. (1990) *Biochim. Biophys. Acta 1020*, 107−111.
84. Takahashi, E., and Wraight, C. A. (1992) *Biochemistry 31*, 855−866.
85. Paddock, M. L., Juth, A., Feher, G., and Okamura, M. Y. (1992) *Biophys. J. 61*, A153.
86. Gunner, M. R., and Honig, B. (1991) *Proc. Natl. Acad. Sci. U.S.A. 88*, 9151−9155.
87. Gopta, O., Bloch, D. A., Cherepanov, D. A., and Mulkidjanian, A. Y. (1997) *FEBS Lett. 412*, 490−494.
88. Oesterhelt, D., and Stoeckenius, W. (1971) *Nature 233*, 149−152.
89. Lanyi, J. K. (1993) *Biochim. Biophys. Acta 1183*, 241−261.
90. Sampogna, R. V., and Honig, B. (1994) *Biophys. J. 66*, 1341−1352.
91. Sampogna, R. V., and Honig, B. (1996) *Biophys. J. 71*, 1165−1171.
92. Bashford, D., and Gerwert, K. (1992) *J. Mol. Biol. 224*, 473−486.
93. Bashford, D., and Karplus, M. (1990) *Biochemistry 29*, 10219−10225.
94. Lancaster, R., and Michel, H. (1997) *Structure 5*, 1339−1359.
95. Kleinfeld, D., Okamura, M. Y., and Feher, G. (1984) *Biochemistry 23*, 5780−5786.
96. Dao-pin, S., Anderson, D. E., Baase, W. A., Dahluist, F. W., and Matthews, B. W. (1991) *Biochemistry 30*, 11521−11529.
97. Stites, W. E., Gittis, A. G., Lattman, E. E., and Shortle, D. (1991) *J. Mol. Biol. 221*, 7−14.
98. Miksovska, J., Maroti, P., Tandori, J., Schiffer, M., Hanson, D. K., and Sebban, P. (1996) *Biochemistry 35*, 15411−15417.
99. Shopes, R. J., and Wraight, C. A. (1985) *Biochim. Biophys. Acta 806*, 348−356.
100. Baciou, L., Sinning, I., and Sebban, P. (1991) *Biochemistry 30*, 9110−9116.
101. Kleinfeld, D., Okamura, M. Y., and Feher, G. (1984) *Biochim. Biophys. Acta 766*, 126−140.
102. Mancino, L. J., Dean, D. P., and Blankenship, R. E. (1984) *Biochim. Biophys. Acta 764*, 46−54.
103. Graige, M. S., Paddock, M. L., Bruce, J. M., Feher, G., and Okamura, M. Y. (1996) *J. Am. Chem. Soc. 118*, 9005−9016.
104. McPherson, P. H., Schonfeld, M., Paddock, M. L., Okamura, M. Y., and Feher, G. (1994) *Biochemistry 33*, 1181−1193.
105. Nabedryk, E., Robles, S. J., Goldman, E., Youvan, D. C., and Breton, J. (1992) *Biochemistry 31*, 10852−10858.
106. Nabedryk, E., Brenton, J., Hienderwadel, R., Fogel, C., Mantele, W., Paddock, M. L., and Okamura, M. Y. (1995) *Biochemistry 34*, 14722−14732.
107. Hienerwadel, R., Grzybek, S., Fogel, C., Kreutz, W., Okamura, M. Y., Paddock, M. L., and Breton, J. (1995) *Biochemistry 34*, 2832−2843.
108. Hienerwadel, R., Nabedryk, E., Paddock, M. L., Rongey, S., Okamura, M. Y., Mäntele, W., and Breton, J. (1992) *Photosynthesis Congress Proceedings*, pp 437−440.
109. Nabedryk, E., Breton, J., Okamura, M. Y., and Paddock, M. L. (1998) *Biochemistry 37*, 14457−14462.
110. Breton, J., and Nabedryk, E. (1998) *Photosynth. Res. 55*, 301−307.
111. Hienerwadel, R., Thibodeau, D., Lenz, F., Nabedryk, E., Breton, J., Kreutz, W., and Mantele, W. (1992) *Biochemistry 31*, 5799−5808.

BI982700A